



1 **Traces of urban forest in temperature and CO₂ signals in** 2 **monsoon East Asia**

3 Keunmin Lee¹, Je-Woo Hong², Jeongwon Kim¹, and Jinkyu Hong¹

4 ¹Department of Atmospheric Sciences, Yonsei University, Seoul, 03722, Korea (Republic of)

5 ²Korea Environment Institute, Sejong, 30147, Korea (Republic of)

6 *Correspondence to:* Jinkyu Hong (jhong@yonsei.ac.kr)

7 **Abstract.** Cities represent a key space for our sustainable trajectory in a changing environment, and our society
8 is steadily embracing urban green space for its role in mitigating heatwaves and anthropogenic CO₂ emissions.
9 This study reports two-year surface fluxes of energy and CO₂ measured via the eddy covariance method in an
10 artificially constructed urban forest to examine the impact of urban forests on air temperature and net CO₂
11 exchange. The urban forest site shows typical seasonal patterns of forest canopies with the seasonal march of the
12 East Asian summer monsoon. Our analysis indicates that the urban forest reduces both the warming trend and
13 urban heat island intensity compared to the adjacent high-rise urban areas and that photosynthetic carbon uptake
14 is large despite relatively small tree density and leaf area index. During the significant drought period in the second
15 year, gross primary production and evapotranspiration decreased, but their reduction was not as significant as
16 those in natural forest canopies. We speculate that forest management practices, such as artificial irrigation and
17 fertilization, enhance vegetation activity. We also stipulate that ecosystem respiration in urban forests is more
18 pronounced than typical natural forests in a similar climate zone. This can be attributed to the substantial amount
19 of soil organic carbon available due to intensive historical soil use and soil transplantation during forest
20 construction, as well as relatively warmer temperatures in urban heat domes. Our observational study also
21 indicates the need for caution in soil management for less CO₂ emissions in urban areas.

23 **1 Introduction**

24 Cities inhabit only 2% of the Earth's land surface but hold more than 55% of the world's population. With the
25 unprecedented rapid urbanization in the last century, our life trajectory heavily depends on urban structures and
26 functions, and it is expected that the urban population will increase by up to 68% by 2050 (UN, 2019). Our current
27 concern is regarding the disastrous impacts of climatic events (e.g., heatwaves, flooding, and drought) and
28 environmental changes (e.g., air pollution and land degradation) on our socioeconomic system in a changing
29 climate (McCarthy et al., 2010; Rahmstorf and Coumou, 2011). Accordingly, it remains an urgent issue to
30 implement integrated policies for climate change mitigation and adaption toward sustainable cities against global
31 warming and related natural disasters. In particular, urban green infrastructures, such as urban forest, have been
32 recognized as a key solution toward alleviating climatic and environmental disasters (e.g., Oke et al., 2017;
33 Chiesura, 2004; Haaland and van den Bosch, 2015; Kroeger et al., 2019). Green spaces in cities, as opposed to
34 gray spaces, are exposed to wide ranges of environmental and climatic conditions across geographical locations.



35 Especially when green spaces replace gray infrastructures during the urban redevelopment, it remains unclear
36 whether their benefits emerge in real conditions and thereby outperforming their maintenance cost and other
37 harmful effects. To leverage their full potential benefits, it is necessary to assess the biophysical effects of urban
38 forests based on direct long-term monitoring in urban areas.

39 Urban forests are a key part of green infrastructures in a city, and two of their benefits, which have been mainly
40 addressed in previous studies, are thermal mitigation and carbon uptake (Roy et al., 2012; Oke et al., 2017). Firstly,
41 urban forests mitigate direct sunlight and diminish the incoming radiant energy on the land surface, thereby
42 reducing surface temperature. Additionally, urban forests supply water to the atmosphere through transpiration
43 and retain water for longer times than the impervious surfaces of urban structures. These processes contribute
44 toward reducing air temperature by partitioning more available energy to latent heat flux (Q_E) than sensible heat
45 flux (Q_H), thus creating favorable conditions for mitigating heatwaves and related health problems (e.g., Oke,
46 1982; Hong et al., 2019a). Eventually, this cooling effect reduces the electrical energy load of buildings, as well
47 as greenhouse gas emissions. Previous studies have reported cooling effects of urban forests from street trees to
48 parks scales (Oke et al., 1989; Bowler et al., 2010; Norton et al., 2015; Shashua-Bar and Hoffman, 2000). Such
49 cooling effects depend not only on tree species and structures (Feyisa et al., 2014) but also on the size and
50 vegetation density of urban green areas (Yu and Hien, 2006; Chang et al., 2007; Hamada and Ohta, 2010; Feyisa
51 et al., 2014). However, despite the strong temperature-controlling factors of evapotranspiration (ET) and direct
52 heat fluxes over urban forest canopies, only a few studies have reported surface energy balance (SEB) in urban
53 forests in relation to thermal mitigation based on direct measurements (e.g., Oke et al., 1989; Spronken-Smith et
54 al., 2000; Coutts et al., 2007a; Ballinas and Barradas, 2015; Hong and Hong, 2016;). Moreover, it is noticeable
55 that forest cooling intensity depends on geography and even forests can produce a warming trend with the
56 decreased albedo (Bonan, 2008; Wang et al., 2018). The lack of direct urban forest measurements hinders proper
57 assessment of their influences on the climate and environment.

58 Furthermore, urban forests mitigate anthropogenic carbon emissions by photosynthetic CO₂ uptake. Traditionally,
59 carbon uptake by urban forests has been estimated by empirical relationships (e.g., biomass allometric equation)
60 or short-term inventory of biomass data and vegetation growth rates, which have limitations of spatiotemporal
61 coverage (Rowntree and Nowak, 1991; Nowak, 1993; Nowak et al., 2008; Weissert et al., 2014). Currently, the
62 eddy covariance (EC) method is being applied in various ecosystems from grasslands and natural forests to urban
63 areas because it provides continuous net CO₂ flux measurements at the neighborhood scale every half hour
64 (Christen 2014). From this perspective, the EC method is useful for studying the net CO₂ exchange (F_C) from
65 diurnal to interannual variations, with its simultaneous measurement of surface energy fluxes. Recently, direct F_C
66 measurements have been performed using the EC method in urban green spaces to examine SEB and carbon
67 exchange (Coutts et al., 2007a, 2007b; Awal et al., 2010; Bergeron and Strachan, 2011; Crawford et al., 2011;
68 Kordowski and Kuttler, 2010; Peters and McFadden, 2012; Velasco et al., 2013; Ward et al., 2013; Ueyama and
69 Ando, 2016; Hong et al., 2019b; Hong et al., 2020). However, the EC method provides only the net effects of CO₂
70 exchange from various carbon sources and sinks, which limits the physical interpretation and assessment of the
71 benefits and costs of urban forests.



72 Flux partitioning into photosynthesis and ecosystem respiration from the EC measured F_C requires additional
73 information and data processing (Stoy et al., 2006). It is more challenging to partition F_C into individual sources
74 and sinks, particularly in urban areas because of the complex contributions from biogenic (e.g., vegetation
75 photosynthesis, respiration of vegetation, soil, and humans) and extra anthropogenic (e.g., fossil fuel combustion
76 by transportation or in households and commercial buildings) processes (Pataki et al., 2003). Stochastic F_C
77 partitioning methods were recently applied by reprocessing EC observation data with auxiliary data and provided
78 useful knowledge on urban carbon cycle (Hiller et al., 2011; Crawford and Christen, 2015; Menzer and McFadden,
79 2017; Stagakis et al., 2019).

80 With this background, the objectives of this study include: 1) reporting temporal changes in air temperature after
81 the artificial construction of an urban forest park in the Seoul metropolitan area where a hot and humid summer
82 season affects and shows steep global warming trends (Hong and Hong, 2016) and 2) quantifying the carbon
83 uptake of urban forests based on the F_C partitioning through the data observed by the EC method and
84 meteorological data (Lee et al., 2021). Here, we highlight the biotic and abiotic factors controlling the carbon
85 cycle in urban forests and the impact of urban forests on the thermal environment after forest park construction.

86 2 Materials and Methods

87 2.1 Urban surface energy and CO₂ balances

88 The SEB is expressed as:

$$89 \quad Q^* + Q_F = Q_H + Q_E + \Delta Q_S + \Delta Q_A \quad (1)$$

90 where Q^* is the net all-wave radiation of the sum of outgoing and incoming short- and long-wave radiative fluxes,
91 Q_F is the anthropogenic heat flux, Q_H is the turbulent sensible heat flux, Q_E is the latent heat flux, ΔQ_S is the net
92 storage heat flux, and ΔQ_A is the net heat advection (Definitions of variables in Appendix A).

93 The surface CO₂ budget in an urban forest is formulated as follows:

$$94 \quad F_C = E_R + E_B + RE - GPP \equiv E_R + E_B + NBE \quad (2)$$

95 where F_C is the net CO₂ exchange at the city-atmosphere interface, E_R and E_B are the anthropogenic CO₂ emissions
96 from fossil fuel combustion by vehicles and heating in a building, respectively. GPP and RE are biotic
97 contributions to F_C ; GPP is the gross primary production as a result of photosynthetic CO₂ uptake, and RE is the
98 ecosystem respiration from soil and vegetation. Urban ecosystem respiration considers not only the autotrophic
99 and heterotrophic respirations of vegetation and soil but also human respiration (Moriwaki and Kanda, 2004;
100 Velasco and Roth, 2010; Ward et al., 2013, 2015; Hong et al., 2020). Human respiration is negligible in this study
101 because there is no residential population in the park. Vegetation in urban areas includes trees and lawns in urban
102 forests, as well as gardens and roadsides, and it offsets CO₂ emissions through CO₂ assimilation by photosynthesis
103 as the only carbon sink.



104 Additionally, NBE is the net biome CO_2 exchange and is typically defined as the net ecosystem exchange by RE
105 $- GPP$ for natural vegetation. Put differently, NBE refers to carbon losses in heterotrophic respiration minus the
106 net primary production on natural vegetative surfaces; thus, negative NBE indicates the net carbon uptake by the
107 natural ecosystem (Kirschbaum et al., 2001; Randerson et al., 2002). Unlike natural ecosystems, the F_C between
108 an urban forest and atmosphere is a complex mixture of biogenic (i.e., GPP and RE) and anthropogenic (i.e., E_R
109 and E_B) processes across various spatial and temporal scales. In urban environments, anthropogenic emissions
110 depend on the local characteristics (e.g., climate, population density, levels of industrial activity, and existing
111 carbon intensity of electricity supply) of the city and locations of the eddy covariance system (Feigenwinter et al.,
112 2012; Kennedy et al., 2014; Lietzke et al., 2015; Stagakis et al., 2019).

113

114 2.2 Site description

115 2.2.1 Seoul Forest Park

116 Micrometeorological measurements were taken at the Seoul Forest Park (SFP) in the Seoul metropolitan area,
117 Korea (37.5446°N, 127.0379°E). SFP is the third largest park in Seoul with an area of 1.16 km² (Fig. 1a). This
118 area had been used as a horse racetrack and a golf course inside the track since 1950 and was surrounded by
119 cement factories to the west (Fig. 1b). The local government initially planned this area as a commercial district
120 with a high-rise multi-purpose building complex but changed its plan to redevelop the area as a green space in
121 late 1990s. The construction of the SFP began in December 2003, and it was opened to the public in June 2005
122 (Fig. 1c).

123 The dominant land cover within a 300-m radius of the measurement system is a deciduous forest with irrigated
124 grass lawns (*Zoysia*), oak (*Quercus acutissima*), ginkgo (*Ginkgo biloba*), and ash trees (*Fraxinus rhynchophylla*),
125 which correspond to the Local Climate Zone (LCZ) ‘A’, dense trees (Stewart and Oke, 2012). The maximum leaf
126 area index (LAI) of 300 × 300 m² around the SFP tower is approximately 1.6 (Copernicus Service information,
127 2020). On the east side (0–120°), there are trees (approximately 230 stems ha⁻¹) with a small artificial lake and
128 grasslands beyond it. Trees mainly occupy the southern and western directions of a tower (120–330°) within a
129 100-m radius area (approximately 540 stems ha⁻¹) and traffic roads lie outside of the dense vegetation. The mean
130 tree height (h_c) is approximately 7.5 m and ranges between 5.8–9.5 m. The mean roughness length (z_0) and zero-
131 plane displacement height (z_d) are estimated by the tree height-based approach within 100 m radius and they range
132 between 0.3–0.6 and 4.1–8.2 m, respectively (Raupach et al., 1991). z_0 and z_d have seasonal and directional
133 variations depending on the variability of the leaves on the vegetation (Lee, 2015; Kent et al., 2018). z_0 and z_d
134 change from approximately 0.6 and 5.0 m during leaf-on period (June–August) to 1.2 and 3.0 m during the leaf-
135 off periods (December–February) by the Macdonald method (Macdonald et al., 1998). Approximately 80% of the
136 footprint area of the SFP tower is within 250 m (Fig. 1e).

137 The traffic roads consist of eight and ten lanes carrying heavy traffic throughout the day (~100,000 vehicles day⁻¹)
138 to the south and west of the tower (Fig. 1c). Hourly traffic volume, which is used for surface flux partitioning,
139 is evaluated on the road adjacent to the SFP tower every year by the Seoul Metropolitan Government



140 (<https://topis.seoul.go.kr>). Across the road on the western side of the tower, a cement factory still exists, although
141 its size is smaller than it used to be in the past (Fig. 1b and 1c).

142 2.2.2 Climate conditions

143 Climatic condition shows a distinct seasonal variation with the seasonal march of the East Asian summer monsoon.
144 The mean climatological values (1981–2010) of the screen-level air temperature (T_{air}) and precipitation were
145 12.5°C and 1450 mm year⁻¹, respectively. During the study period (June 2013–May 2015), the observed T_{air} was
146 higher than the climatological mean. Higher temperatures lasted longer in the summer of 2013 with the stagnation
147 of the migratory anticyclones (June) and North Pacific anticyclone (July–August). There were strong heatwaves
148 in the spring seasons of 2014 and 2015 (Hong et al., 2019a).

149 Notably, seasonal precipitation shows a contrasting pattern between two consecutive years (Fig. 2d). In the first
150 year (June 2013–May 2014), annual precipitation was 1256 mm, which corresponded to approximately 90% of
151 the climatological mean. In addition, approximately 50% of the annual rainfall was concentrated in the summer
152 with an estimated 650 mm occurring only in July 2013; however, in the second year the annual rainfall was 932
153 mm (i.e., 67% of the climatological mean). The monthly precipitation values in the July and August of 2014 were
154 198 and 169 mm, respectively, which represented only approximately 35% of the climate mean. Accordingly, the
155 vapor pressure deficit (VPD) and downward shortwave radiation (K_t) in July 2013 were relatively smaller than
156 those in July 2014 (Fig. 2b and 2c).

157 2.2.3 Observations in the Seoul Metropolitan Area

158 In this study, meteorological data from six stations (one eddy covariance station, one aerodrome meteorological
159 observation station, and four automatic weather stations) in the Seoul Metropolitan Area are additionally analyzed
160 to examine the heat mitigation and CO₂ reduction effects of urban vegetation in the SFP (Table 1 and Fig. 1a).
161 The Eunpyeong eddy covariance site (EP, 37.6350°N, 126.9287°E) is for surface flux observations in the
162 northwest of Seoul, where there was a recent urban redevelopment to high-rise and high-population residential
163 areas from low-rise areas (Hong and Hong, 2016; Hong et al., 2019b). Flux observations at the site have been
164 conducted since 2012, and they show the SEB and turbulence characteristics of a typical urban residential area.
165 Because the area around the SFP was originally planned to be redeveloped to high-rise high-population residential
166 buildings, EP is selected for comparative analysis as a hypothetical place for the SFP region because they are
167 close to each other and so have the similar synoptic conditions.

168 The Gimpo Airport Observatory (GP, 37.5722°N, 126.7751°E) is located on the western boundary of Seoul, and
169 it is surrounded by grasslands and croplands, which corresponds to LCZ ‘D’. As the dominant wind comes from
170 the west, the GP site is generally affected by the same synoptic weather conditions as Seoul. The GP station
171 represents the rural environment of the Seoul Metropolitan Area because urban development is restricted around
172 the airport (Hong et al., 2019a). In this study, we select the GP site as a reference point and calculate the urban
173 heat island intensity (UHI) as the synchronous difference in T_{air} between the urban and rural areas accordingly
174 (Stewart, 2011).



175 The Seongdong Observatory (SD, 37.5472°N, 127.0389°E), the closest station to the SFP, is located
176 approximately 300 m north of the SFP tower (Fig. 1c). Since the station began observations in August 2000, the
177 meteorological data at SD are useful for analyzing temperature changes before and after the construction of the
178 SFP. Accordingly, it is used to analyze local climatic changes caused by the SFP. Moreover, SD provides auxiliary
179 weather variables (e.g., precipitation) that are not observed in SFP station and reference data for surface flux gap
180 filling. The Gangnam, Seocho, and Songpa observatories (hereafter denoted as AVG) are located in Seoul's
181 central business district, which corresponds to LCZ 1 or 2. These sites are also close to the SFP (~ 5 km); thus,
182 temperatures in these regions can be assumed to be exposed to the same synoptic condition. These regions show
183 greater UHI than other parts of Seoul because of dense skyscrapers, according to the analysis of the spatial
184 distribution of UHI in Seoul (Hong et al., 2013). The average temperature of these three automatic weather
185 stations is used to evaluate the temperature and UHI reduction effects of the SFP construction. All meteorological
186 data from the automatic weather station and aerodrome meteorological observation station are observed every
187 minute, and they are averaged for 1 h for UHI analysis. All the meteorological data are processed for quality
188 control on the National Climate Data Portal of the Korea Meteorological Administration (<http://data.kma.go.kr>).

189 2.3 Instrumentation and data processing

190 The measurement system was installed on the rooftop of the SFP facility building (Fig. 1d). A three-dimensional
191 sonic anemometer (CSAT3A, Campbell Scientific, USA) and enclosed infrared gas analyzer (EC155, Campbell
192 Scientific, USA) were mounted 12.2 m above the ground level (2.8 m above the roof of an 8.4 m high building)
193 for 2 years (Fig. 1d). The eddy covariance data were recorded using the data logger (CR3000, Campbell Scientific,
194 USA) with a 10-Hz sampling rate and a 30-min averaging time. The gas analyzer was calibrated with standard
195 CO₂ gas every three months. The main footprint covered the forest canopies, and the measurement height (z_m)
196 satisfied the tower height requirement over forested or more structurally complex ecosystems (i.e., $z_m \cong z_d + 4(h_c$
197 $- z_d)$) (Munger et al., 2012). Two radiometers (NR Lite2 and CMP3, Kipp&Zonen, Netherlands) were used to
198 measure the radiative fluxes. An auxiliary measurement included a humidity and temperature probe (HMP155A,
199 Vaisala, Finland).

200 The 30-min flux is computed using EddyPro (6.2.0 version, LI-COR), with the applications of the double rotation,
201 time lag compensation using covariance maximization, spike removal and quality test (Vickers and Mahrt, 1997),
202 spectral corrections for low-frequency (Moncrieff et al., 2004) and high-frequency (Fratini et al., 2012), as well
203 as vertical sensor separation correction (Horst and Lenschow, 2009). We apply the following post processes for
204 quality control: 1) plausible value check, 2) spike removal, and 3) discarding the negative F_C flux during the
205 nighttime (Hong et al., 2020). The total study period from installation (31 May, 2013) to termination (03 June,
206 2015) is approximately 2 years (35,174 potential 30-min data), and the total available data are approximately
207 90.1%, 88.3%, and 85.4% ($n = 31709, 31064, 30028$) for Q_H , Q_E , and F_C after the processes, respectively.

208 It is important to partition the F_C into four contributing components (i.e., RE , GPP , E_R , and E_B in Eq. 2) to
209 investigate their biotic and abiotic controlling factors in an artificially constructed park. This study applies for a



210 statistical partitioning method described in Lee et al. (2021). More information and relevant figures on the flux
211 partitioning are available in Lee et al. (2021).

212 3 Results and discussion

213 3.1 Surface energy balance

214 The SEB at the SFP shows typical seasonal variations over natural forest canopies with the seasonal march of the
215 East Asian monsoon (Fig. 4) (Hong and Kim, 2011; Hong et al., 2019b; Hong et al., 2020). In summer, there are
216 lengthy rainy spells and large temporal variabilities of meteorological conditions with the impacts of the East
217 Asian summer monsoon (Fig. 2d). This heavy rainfall causes substantial decreases in K_1 , and thus Q^* , with large
218 temporal variations, thereby leading to the mid-summer depression of surface fluxes (Fig. 2c and 4). Q^* also
219 reaches its maximum in spring rather than in summer and decreases gradually from spring to winter (Fig. 4). More
220 than half of Q^* is partitioned to Q_E , and Q_H is minimum in summer owing to the ample water supply from the
221 summer rainfall. However, Q_H is maximum in spring and even larger in winter, despite the relatively smaller Q^* ,
222 because of the cold and dry climatic conditions induced by the winter monsoon. Accordingly, the seasonal mean
223 Bowen ratio ($\beta = \sum Q_H / \sum Q_E$) ranges from near zero (summer) to approximately 4 (winter) with its daily maximum
224 around 9 in early January 2015 (Fig. 5). Notably, β in the SFP is consistently lower than the high-rise, high-density
225 residential area (i.e., the EP site) because of the ET from the vegetative canopies and the unpaved surfaces in the
226 urban forest. This difference between the two distinct sites confirms that urban forests are responsible for
227 substantial changes in the thermal environment in terms of Q_H and Q_E , as well as their related air and surface
228 temperatures because of more evaporative cooling in green spaces compared to impervious surfaces such as roads
229 and buildings in urban areas (Oke et al., 2017).

230 The SEB also shows interannual variabilities over forest canopies influenced by the timing of the onset and
231 duration of the summer monsoon (Hong and Kim, 2011) (Fig. 6). As discussed in Section 2.1.2, annual
232 precipitation is much larger in the first year than in the second year because of the interannual variations in the
233 East Asian monsoon activity, thereby making substantial differences in surface radiative fluxes. Furthermore, Q_E
234 shows the difference between the first and second years of the observation, particularly by responding to such
235 interannual variability of radiation. In the first year of the observation, Q_E is more than 300 W m^{-2} and has a
236 relatively larger temporal variability because of the frequent rainfall events in summer, compared to the second
237 year.

238 Evapotranspiration rate ranges from 5 mm month^{-1} in January 2015 to 74 mm month^{-1} in August 2013, and the
239 annual ET values are 367 and 320 mm year^{-1} in the first and second years, respectively (Fig. 5 and Table. 2). The
240 ET values correspond to 29.3% and 34.3% of the annual precipitations (Fig. 2d). The difference in ET between
241 the two consecutive years (i.e., 48 mm) mainly occurred in summer (42 mm), especially in August (30 mm). It
242 has been reported that approximately 55% of the net radiation is partitioned to latent heat flux in forest canopies
243 globally (Falge et al., 2001; Suyker and Verma, 2008). The annual ET to net radiation from the urban forest is
244 smaller than this global average and it is also smaller than that of forests at similar latitudes in the East Asia



245 (Khatun et al., 2011). The annual ET in the second year is smaller than that in the first year with extensive drought
246 in the second year. However, it is notable that the ET in the second year shows only an approximately 12%
247 decrease compared to the first year, despite a substantial decrease in precipitation (26% decrease) and similar net
248 radiation (Table 2). Although the summer monsoon provides ample water to the ecosystem, its delay and weakness
249 result in severe drought and stress to the ecosystem in this region (Hong and Kim, 2011); however, such ecosystem
250 stress, such as the shrinking of ET and carbon uptake, is inexplicit for the urban forest. We speculate that artificial
251 irrigation by a sprinkler mitigated ecosystem stress to a certain degree in the urban forest.

252 3.2 Air temperature

253 Figure 6 shows the mean diurnal pattern of the air temperature difference between the AVG and SD near the SFP
254 ($\Delta T_{air} \equiv T_{air_AVG} - T_{air_SD}$ hereafter) before and after the park construction in summer. Notably, ΔT_{air} is always
255 positive during the entire summer season (i.e., AVG is warmer than SD) and shows distinct impacts in terms of
256 magnitude and diurnal variations after the park construction. The warming trend is evident at the AVG ($p < 0.015$),
257 wherein there were no changes in the urban structure and function around them. The warming rate at the AVG is
258 $3.0 \text{ }^\circ\text{C century}^{-1}$, which corresponds to the warming rate reported in the high-rise urban area in Seoul (Hong et al.,
259 2019a). However, the warming rate around the SFP is approximately $1.6 \text{ }^\circ\text{C century}^{-1}$, which is smaller than that
260 of the AVG and other urban areas in Seoul and is comparable to the global mean warming rate of $0.9 \text{ }^\circ\text{C century}^{-1}$
261 (Hansen et al., 2010; Hong et al., 2019a).

262 Notably, such a lower warming trend around the SFP mainly occurs in the afternoon when ET is dominant. This
263 difference will be larger if we consider that the measurement height at the AVG is higher than that at the SD
264 (Table. 1). The maximum ΔT_{air} is approximately $0.3 \text{ }^\circ\text{C}$ around 10:00 before the park construction (Fig. 6a) and
265 increases up to approximately $0.5 \text{ }^\circ\text{C}$ with its peak occurrence shifting from the morning to the afternoon (i.e.,
266 around 14:00) after the construction (Fig. 6b). This peak time in the afternoon is coincident with the time when
267 photosynthesis is the highest in the vegetation; thus, Q_E increases in summer. Our results indicate that the thermal
268 mitigation of the urban forest is important as a result of increases in ET, especially if we consider that the SFP
269 area was originally planned to be developed as a high-population multipurpose building complex.

270 3.3 Urban heat island intensity

271 The influence of urban forests on summer temperature produces also evident traces in UHI. Figure 7 shows the
272 mean diurnal variation of UHI at the SFP and AVG during summer. Apparently, the UHI of the SFP (UHI^S
273 hereafter) and AVG (UHI^A hereafter) gradually increases after mid-afternoon and is the largest at night. This
274 diurnal pattern is consistent with previous reports in cities exposed to different geographical and climatic
275 conditions because rural areas cool faster than urban areas (Oke et al., 2017). Additionally, UHI^A is positive
276 throughout all days ranging from $0.2\text{--}2.2 \text{ }^\circ\text{C}$ (i.e., warmer than rural area, GP) and is greater than UHI^S by 0--
277 $1.5 \text{ }^\circ\text{C}$. A possible reason for this stronger UHI^A is that the AVG stations are located in the central business
278 district; thus, the densities of buildings surrounding these stations are much higher than those surrounding the SFP



279 station. At night (19:00–06:00), UHI^{A} and UHI^{S} are approximately 1.8 °C and 1.4 °C, respectively. The maximum
280 UHI difference between the AVG and SFP was 0.7 °C in 2013 and 0.5 °C in 2014.

281 Around sunrise, sharp declines in the UHI are observed because the air temperature near the urban area increases
282 relatively slowly as urban fabrics, such as asphalt, brick, and concrete, have larger heat capacities and less sky
283 view factors than the rural areas (Oke et al., 2017). Eventually, this slow increase in the air temperature reduces
284 the differences in T_{air} among the stations, thereby reducing the UHI . The minimum UHI^{A} values were 0.3 °C
285 (2013) at 09:30 and 0.2 °C (2014) at 08:30, while the minimum UHI^{S} occurs at 10:30 with values of –0.1 °C
286 (2013) and 0.0 °C (2014). This implies that the timing of the minimum UHI is delayed in the SFP compared to
287 the AVG. Our findings indicate that the urban forest has a similar air temperature in the daytime as compared to
288 the rural area (i.e., GP) where has a lower thermal admittance because of its location within the airport. Especially
289 when there is strong ET and more time is required to warm the SFP surface, the urban-rural difference in thermal
290 admittance becomes relatively small. This can be attributed to the higher thermal capacity of the wetter soil of the
291 SFP as a result of artificial irrigation and the absence of impervious surfaces (Oke et al., 1991).

292 The diurnal variations in UHI^{S} also show the interannual variability in both amplitude and steepness over the two
293 consecutive years. Despite the similar summertime UHI^{A} for both years, the daytime UHI^{S} in 2013 was
294 approximately 0.2 °C lower than that in 2014. Notably, the summer Q_E was greater in 2013 than in 2014, and this
295 observed summertime asymmetric difference between the SFP and AVG stations was not found in the winter
296 when ET was negligible (not shown here).

297 Our results suggest that urban forests can play a significant role in mitigating the thermal environment because of
298 the wetter soil surface of the park and subsequent increases in Q_E , compared to the impervious surfaces in urban
299 areas. In particular, our findings indicate that the heat mitigation of the urban forest depends on the ratio of Q_E to
300 net radiation. Indeed, there is an evident negative relationship between daytime Q_E and air temperature differences
301 between the SFP and AVG stations (Fig. 8). As K_1 is more partitioned to Q_E , T_{air} of the SFP decreases more than
302 that of the AVG, and the maximum temperature difference is observed in the summer season. The SFP is cooler
303 than the AVG by up to 0.6 °C, but the SFP is warmer than the AVG during the winter-dormant season when ET
304 is small.

305 3.4 Temporal dynamics of net CO₂ exchange

306 Figure 9 shows the diurnal evolution of F_C and footprint-weighted road fraction (λ). Overall, the mean daytime
307 F_C is negative (i.e., carbon uptake) in the summer (June–August), indicating that photosynthesis, the only carbon
308 sink, is dominant. This carbon uptake period is coincident with the active vegetation manifested by increases in
309 EVI (not shown here). Summertime photosynthetic carbon uptake (GPP) has a daily average of 7.6 $\mu\text{mol m}^{-2} \text{s}^{-1}$
310 with a maximum of 18.9 $\mu\text{mol m}^{-2} \text{s}^{-1}$ around 12:30 (Fig. 8a in Lee et al., 2021). A daily minimum F_C also occurs
311 around 12:30 with the maximum photosynthetic carbon uptake during this time accordingly. The vegetation
312 around the SFP absorbs more CO₂ than carbon sources and F_C becomes negative only during the summer daytime.
313 However, because of substantial amounts of anthropogenic emissions and ecosystem respiration, F_C changes from



314 negative (i.e., carbon sink) to positive values (i.e., carbon source) even around 16:30 in summer unlike in natural
315 ecosystems, despite the substantial downward shortwave.

316 CO₂ uptake is highest in June, with a maximum of approximately 13 μmol m⁻² s⁻¹ (Fig. 9a). In the middle of
317 summer (4th and 31st two-week data in Fig. 9a), CO₂ uptake decreases significantly because photosynthesis is
318 limited because of the reduced K_1 by cloud and rainfall with the onset of the summer monsoon (Fig. 2c). This
319 mid-summer depression of carbon uptake has been reported in the Asian natural vegetations (e.g., Kwon et al.,
320 2009; Hong and Kim, 2011; Hong et al., 2014). Higher reduction in CO₂ uptake observed in 2013 than in 2014
321 was attributed to a longer monsoon period in 2013. Indeed, from 8 to 21 July 2013 (4th two-week data in Fig. 9a),
322 the accumulated precipitation was approximately 400 mm for two weeks, and the daily averaged K_1 was only 70
323 W m⁻².

324 As photosynthesis decreases, F_C changed to positive values from November. During the non-growing season (i.e.,
325 late autumn, winter, and early spring), anthropogenic emissions were also dominant because photosynthesis and
326 ecosystem respiration decrease with smaller K_1 and lower temperatures. During these periods, F_C had minimum
327 values at 04:00–05:00 and increases until 15:00–16:00. Therefore, the diurnal variations in F_C mainly followed
328 the traffic volume (Fig. 4a in Lee et al., 2021), and there also is a clear positive relationship between F_C and λ
329 (23rd, 45th, and 47th two-week data in Fig. 9). It is also noteworthy that the peak time of F_C (16:00) is earlier
330 than the peak time of λ (18:00) from December to early March because E_B is the largest at around 15:00–16:00,
331 indicating that E_R and E_B are the controlling factor of F_C in this period.

332 With such apparent seasonal F_C variation, it is notable that its variability depends on the spatio-temporal
333 distribution of CO₂ sources and flux source area because the latter covers various land use with changes in wind
334 direction and atmospheric stability (Fig. 10). In autumn, the main wind direction changed to the north as the
335 synoptic conditions change particularly (Fig. 3); therefore, λ is smaller in autumn compared to other seasons (Fig.
336 9b). For example, the road fraction was smallest at < 1% from midnight to midday and < 3% during the afternoon
337 in October and November (11th, 12th, 36th, and 37th two-week data in Fig. 9b). In these periods, the nighttime
338 F_C showed the lowest value of approximately 2.9 μmol m⁻² s⁻¹, which was attributable to the smallest road fraction,
339 lower respiration, and minimal heating usage.

340 In early spring, λ was generally larger; thus, E_R played a significant role in F_C , and E_B also remained non-zero
341 until early April, thereby resulting in the largest F_C in this period. With a shutdown of the heating system (i.e.,
342 zero E_B) and the sprouting of leaves in April, there was a sharp decrease in F_C (Fig. 10b and 10c). From December
343 to March, CO₂ emissions increased up to 30 μmol m⁻² s⁻¹ with larger variability in the south–west direction because
344 of intermittent anthropogenic emissions from the park facility (due to space heating and boiling water), as well as
345 the relatively increased contribution of vehicles on the road in the western part of the site.

346 Although the positive F_C in the winter decreased in spring, its magnitude showed directional differences (Fig.
347 10c). On the eastern side, the mean F_C showed a negative value in May, whereas it remained positive on the
348 western side (210–270°) until May. Therefore, these findings further indicating the different contributions of



349 various carbon sources and sinks among the different wind directions. For the wind directions from the north to
350 the east (0–120°), F_C showed a relatively weaker carbon sink than other directions because of the relatively low
351 tree fraction in this direction (Fig. 10a and 10c). On the southern side (150–180°) having the highest tree cover
352 fraction, a maximum carbon uptake about $15 \mu\text{mol m}^{-2} \text{s}^{-1}$ on average was found in June. However, despite the
353 dense vegetation on the south and west side (120–330°), the F_C magnitude was much smaller than that of other
354 natural forests. This is related to the anthropogenic emissions from vehicles on the roads which is discussed in
355 section 3.6.

356 3.5 Light use efficiency of biogenic CO₂ components

357 F_C at the SFP shows a typical light response to the photosynthetically active radiation (PAR) in a way similar to
358 natural ecosystems in spite of anthropogenic CO₂ sources from vehicles (Fig. 11a and 11b). However, this light
359 response in the urban forest is a distinct contrast with the non-dependent F_C in high-rise high-population
360 residential areas in Seoul under the same climatic conditions (EP station). Importantly, GPP , NBE , and F_C show
361 different trends on PAR depending on the direction. As stated in Section 2.1.1 and 3.4, the western side has a
362 higher density of trees as against more grass on the eastern side, and biotic CO₂ uptake from the western side is
363 substantially larger than that on the eastern side. Accordingly, the slope of the light response curve for PAR on
364 the western side is steeper than on the eastern side. F_C at zero PAR ($F_{C,0}$) is larger on the western side ($9.7 \mu\text{mol}$
365 $\text{m}^{-2} \text{s}^{-1}$) than on the eastern side ($5.1 \mu\text{mol m}^{-2} \text{s}^{-1}$) because of a contribution of E_R from roads on the western side
366 of the tower.

367 NBE shows a comparable light response to natural vegetation (e.g., Schmid et al., 2003). A rectangular hyperbolic
368 equation has been used to examine the light response of NBE and elucidate the directional differences in carbon
369 uptake:

$$370 \quad NBE = -GPP + RE = -\frac{\alpha \cdot GPP_{sat} \cdot PAR}{GPP_{sat} + \alpha \cdot PAR} + RE \quad (3)$$

371 where α is the quantum yield efficiency (the initial slope of the light-response curve), GPP_{sat} is the potential rate
372 of the ecosystem CO₂ uptake. α is approximately 0.0651 and $0.0558 \mu\text{mol CO}_2 (\mu\text{mol photon})^{-1}$ on the western
373 and eastern sides, respectively. Notably, α on the western side is comparable to the high initial quantum yield in
374 crops and subtropical forests in East Asia (Hong et al., 2019b; Emmel et al., 2020). Additionally, GPP_{sat} is 30.9
375 and $12.7 \mu\text{mol m}^{-2} \text{s}^{-1}$ on the western and eastern sides, respectively. In addition, the light saturation points are at
376 a PAR of $1500 \mu\text{mol m}^{-2} \text{s}^{-1}$ on the eastern side, which occur at a relatively lower PAR than on the western side.
377 Daytime respiration estimated from equation (3) is 6.7 and $6.3 \mu\text{mol m}^{-2} \text{s}^{-1}$ on the western and eastern sides,
378 respectively. Because GPP is related to PAR, the difference in monthly cumulative GPP between the two years
379 shows a close relationship with the difference in the monthly sunshine duration ($r^2 = 0.75$, not shown here), thereby
380 suggesting a possible impact of change in the onset of the summer monsoon on urban forests.

381 The magnitude of NBE from the western side is larger than that from the suburban area having about 50%
382 vegetative fraction in Montreal, Canada (Fig. 7b in Bergeron and Strachan, 2011) and F_C from a highly vegetated



383 environment of about 67% vegetative fraction in Baltimore, USA (Crawford et al., 2011). Also, *GPP* from the
384 western side is comparable to the dense forest canopies in subtropical forests in Korea (Hong et al., 2019b),
385 deciduous forest ecosystems (Goulden et al., 1996), and a mixed hardwood forest ecosystem (Schmid et al., 2000).
386 However, *NBE* from the eastern side is similar to *F_C* from the suburban areas of about 44%, 50%, and 64%
387 vegetative fraction in Swindon, UK (Ward et al., 2013) and Montreal, Canada (Bergeron and Strachan, 2011), and
388 Ochang, Korea in the same climate zone (Hong et al., 2019b), respectively.

389 3.6 Annual budget of CO₂ sources and sink

390 The annual budget of the *F_C* and its components is summarized in Table 3. The annual sums of the *GPP* and *RE*
391 in the SFP are 4.6 kg CO₂ m⁻² year⁻¹ (1244 gC m⁻² year⁻¹) and 5.1 kg CO₂ m⁻² year⁻¹ (1378 gC m⁻² year⁻¹),
392 respectively. This photosynthetic carbon uptake is smaller than its global mean *GPP* in natural deciduous
393 broadleaf forests with similar annual precipitation and annual mean air temperature (total 8 years of data from 4
394 sites of FLUXNET2015 dataset reported in Pastorello et al., 2020) and similar to that of deciduous broadleaf
395 forests in East Asia (Awal et al., 2010; Kwon et al., 2010) (Table 4). Our speculation is, however, that this *GPP*
396 is relatively larger if we consider the low vegetation fraction and leaf area index (LAI) at our urban park. Indeed,
397 *GPP* is comparable to values reported in other urban sites if it is scaled with the vegetation cover fraction. Previous
398 studies have shown that the *GPP* of urban vegetation is scaled with vegetation cover fraction with an increase of
399 about 0.7 kg CO₂ m⁻² year⁻¹ per 10% increase in vegetation cover fraction (Awal et al., 2010; Crawford and
400 Christen, 2015; Velasco et al., 2016; Menzer and McFadden, 2017). *GPP* at the SFP with a 46.6% vegetation
401 cover fraction is approximately 1.5 kg CO₂ m⁻² year⁻¹ larger than this scale (Fig. 12a).

402 Eventually, this large *GPP* results in a substantial decrease in *F_C* when they are scaled by vegetation fraction.
403 Hong et al. (2019b) reported a linear decrease in *F_C* of approximately 3.0 kg CO₂ m⁻² year⁻¹ per 10% increase in
404 vegetation cover fraction based on the observed *F_C* across an urbanization gradient in Korea (Fig. 12b). The annual
405 *F_C* in the SFP of 7.1 kg CO₂ m⁻² is 1.2 kg CO₂ m⁻² year⁻¹ smaller than this scaled relationship (i.e., more carbon
406 uptake). In particular, *F_C* in the SFP is approximately 3.0 kg CO₂ m⁻² year⁻¹ less than that in recently developed
407 high-rise high-population urban areas in Seoul. Our results suggest that efficient management of urban forests,
408 such as regular irrigation and fertilization, can be an efficient way to adapt and mitigate climate change by
409 increasing CO₂ uptake in artificial forest constructions in East Asia.

410 Meanwhile, *RE* at our site is much larger than that in temperate deciduous forests in East Asia (Takanashi et al.,
411 2005; Kwon et al., 2010) and similar to that in the urban forest in East Asia (Awal et al., 2010), as well as to the
412 global mean *RE* over forests with similar annual precipitation and annual mean air temperatures (Pastorello et al.,
413 2020). Put differently, the urban forest considered in our study is an outlier compared to other natural forest
414 canopies and urban forests because $RE/GPP > 1$ (Table 4). Autotrophic respiration is considered to be
415 approximately half of *GPP* as a rule of thumb (Piao et al., 2010), which corresponds to approximately 45% of the
416 *RE* at our site, thereby indicating a large contribution of heterotrophic respiration to *RE*. Indeed, it was reported
417 that soil respiration at the same site was approximately 4 kg CO₂ m⁻² year⁻¹ (Bae and Ryu, 2017). The reason for
418 the large soil organic carbon was mainly because rice cultivation was carried out in this region before the 1950s,



419 and organic carbon-rich soil was transplanted during the SFP construction, and fertilizers were applied regularly.
420 It has also been reported that RE is enhanced in urban areas because of the relatively warmer temperature in urban
421 regions (i.e., UHI) (Awal et al., 2010). Notably, Q_{10} (the rate by which respiration is multiplied when temperature
422 increases by 10 °C) is about 1.9 at the site and matches the Q_{10} value for ecosystem respiration (2.2 ± 0.7)
423 calculated for natural forests across 42 FLUXNET sites (Mahecha et al., 2010). Further analysis based on the
424 observed Q_{10} and the UHI at the SFP indicates that UHI leads to an approximately 5% increase in RE .

425 Figure 13 shows the monthly cumulative sum of the F_C and its partitioned components. Seasonal variations in the
426 strength of carbon sources and sink as well as F_C are mainly regulated by the biogenic component in summer and
427 the anthropogenic component in winter. Furthermore, F_C is minimum in June, despite the similar GPP from June
428 to August because of the relatively smaller RE during the summer season. Even in summer, photosynthetic carbon
429 uptake is balanced with ecosystem respiration and does not offset all biotic and anthropogenic emissions, thus
430 resulting in positive F_C values throughout the year. In winter, E_B is dominant with negligible GPP and RE due to
431 cold temperatures, and E_R also becomes larger than RE from November. E_R shows apparent seasonal variation in
432 wind direction and atmospheric stability. Its magnitude is about $0.0666 \mu\text{mol m}^{-2} \text{veh}^{-1} \text{h s}^{-1}$ in neutral condition
433 and consistent with the value in the inventory data (Lee et al., 2021). The average monthly traffic speed for the
434 road in front of the SFP is $50\text{--}60 \text{ km h}^{-1}$ (based on the January 2014 data from the Seoul Metropolitan Government
435 Traffic Speed Report), and the CO_2 emission rate is approximately $150 \text{ g CO}_2 \text{ km}^{-1} \text{veh}^{-1}$ based on the emission
436 data at this speed (Kim et al., 2011). With the width of the ten-lane road ($25\text{--}30 \text{ m}$), the inventory-based slope
437 (i.e., CO_2 emission rate per vehicle per area per half-hour) is approximately in the range of $0.0631\text{--}0.0757 \mu\text{mol}$
438 $\text{m}^{-2} \text{veh}^{-1} \text{half-hour s}^{-1}$ ($\cong 150 \text{ gCO}_2 \text{ km}^{-1} \text{veh}^{-1} \times 1/30$ or $1/25 \text{ m}^{-1} \times 1/44 \text{ mol gCO}_2^{-1} \times 10^{-3} \text{ km m}^{-1} \times 10^6 \mu\text{mol}$
439 $\text{mol}^{-1} \times 1/1800 \text{ half-hour s}^{-1}$).

440 There is an evident yearly difference in individual carbon sources and sink in two consecutive years. E_B is mainly
441 caused by heating buildings and hot water in park facilities using natural gas. Notably, E_B is also smaller in the
442 first year because of the relatively smaller number of park visitors and consequently smaller gas consumption,
443 compared to the second year. Indeed, E_B is highly correlated with gas consumption in SFP during winter on a
444 monthly basis ($R^2 = 0.94$; Fig. 6 in Lee et al., 2021). Eventually, these annual differences lead to a smaller annual
445 mean total F_C in the first year than in the second year (Table 3). However, RE is maximum in the August of the
446 first year, while it is highest in July of the second year because of the interannual variations in air temperature
447 with changes in the timing and duration of the East Asian summer monsoon, of which impacts have also been
448 reported in natural vegetation in the same region (Hong and Kim, 2011; Hong et al., 2019b). In other words, the
449 monthly mean air temperature is highest in August of the first and July of the second year because of the short
450 East Asian monsoon period and drought in July of the second year. However, the GPP in summer is relatively
451 smaller in the first year by the mid-summer depression of solar radiation because of the elongated monsoon period
452 (Fig. 2). However, GPP does not shrink in the second year of significant drought because there is ample water
453 supply by a sprinkler. Our results emphasize the important role of forest management in enhancing carbon uptake
454 and evaporative cooling despite the low vegetation fraction.



455 4 Summary and conclusions

456 This study reported two-year surface fluxes of energy and CO₂ measured by the eddy covariance method while
457 also examining the role of artificially generated urban forests in mitigating air temperature and anthropogenic CO₂
458 emissions. The study area is located in the East Asian monsoon region, characterized by a lengthy summer rainy
459 season. During the measurement period, the second year was contrasted with the first year because of the drought
460 compared to the normal climate condition in the first year. The study region is a park with an artificially planted
461 forest in the Seoul Metropolitan Area. The urban forest had a heavy traffic volume around it and was redeveloped
462 from a racetrack and factory in the mid-2000s. To examine the mitigation of air temperature, this study compared
463 meteorological conditions in the urban forest with the surrounding high-rise high-population urban areas. This
464 study also proposed a statistical CO₂ flux partitioning method based on temporal subsets of flux data and high-
465 resolution footprint-weighted land use data to understand the abiotic and biotic contributions to F_C .

466 Surface energy balance in the SFP is influenced by the summer monsoon, and more energy is distributed to Q_E
467 than Q_H in the summer when vegetation is active, similar to natural forests in this climate zone. Therefore, the
468 Bowen ratio in this urban forest ranges from near 0 (summer) to about 4 (winter), which is lower throughout the
469 year than that of high-rise and high-density residential areas in Seoul. This suggests that the vegetation and
470 unpaved surfaces of urban forests facilitate more evaporative cooling compared to the impervious surfaces in
471 urban areas. Furthermore, ET decreased in the second year when there was a drought, but this drop was not as
472 much as the reduced precipitation if we consider the substantial changes in precipitation and radiative forcing in
473 two consecutive years.

474 It is also evident that the urban forest reduced the warming trend and UHI around the study area. Air temperature
475 in the SFP was lower than the surrounding area, but this coolness was reinforced after the park was created. The
476 warming trend diminished after the construction of the park and was smaller than that in other urban regions in
477 the Seoul Metropolitan Area. In addition, the construction of the park delayed the timing of the maximum
478 temperature difference between the urban forest and high-rise commercial from the morning to the afternoon,
479 coinciding with the timing of the maximum Q_E . The SFP shows a general diurnal UHI variation pattern, which
480 has a higher temperature at night than in rural areas. However, the UHI in SFP is lower by 0.6 °C in summer
481 compared to the surrounding urban area, and the minimum peak time is delayed, possibly because vegetation and
482 permeable soils in SFP have a larger thermal capacity. Notably, UHI decreased more in the partitioning of
483 incoming energy into latent heat fluxes. As a rule of thumb, there was cooling by 0.2 °C compared to the
484 surrounding urban area if Q_E/K_1 increased by 10%.

485 Net CO₂ exchange at the urban forest showed typical temporal variations in natural forest canopies influenced by
486 the East Asian summer monsoon (Hong and Kim, 2011; Hong et al., 2019b). A mid-summer depression of carbon
487 uptake was observed with the onset of the summer monsoon, like vegetation in the East Asian monsoon region.
488 The GPP was estimated by the statistical partitioning method, and the non-zero GPP period was coincident with
489 the active vegetation of the significant vegetation index. Summertime photosynthetic carbon uptake had a daily
490 average of 7.6 μmol m⁻² s⁻¹ with a maximum of 18.9 μmol m⁻² s⁻¹ around 12:30. However, even during the growing



491 season, vegetative carbon uptake was insufficient to offset anthropogenic CO₂ emissions and ecosystem
492 respiration on a time scale of > 1 day. Our estimations of anthropogenic CO₂ emissions from vehicles and
493 buildings agreed with the estimations based on inventory data such as CO₂ emission rate of vehicles and monthly
494 gas consumption, and their annual budgets each had a comparable magnitude to *GPP*.

495 Annual *GPP* of the urban forest was relatively smaller than that of the forest in East Asia exposed to similar
496 climatic conditions because of the relatively smaller vegetation cover fraction and LAI. However, it was larger
497 than the *GPP* expected from the relationship from previous urban studies if it was normalized by the vegetation
498 cover fraction. *RE* is, however, much larger than that in the temperate East Asian forests and similar to the urban
499 forest in East Asia. We speculate that soil respiration enhanced such large ecosystem respiration by relatively
500 warmer temperatures in a city and rich soil organic carbon in the SFP. Eventually, the annual mean total *F_C* is 7.1
501 kg CO₂ m⁻² year⁻¹, which is smaller than the estimate from the scaling between annual total *F_C* and vegetation
502 fraction (Hong et al., 2019b). Because of the spatial heterogeneity, *F_C* and its components showed directional
503 changes. *NBE* from the eastern side is similar to *F_C* of suburban areas with approximately 44%, 50%, and 64%
504 vegetative fraction in Swindon, UK (Ward et al., 2013) and Montreal, Canada (Bergeron and Strachan, 2011), and
505 Ochang, Korea in the same climate zone (Hong et al., 2019b), respectively. However, the *NBE* and *GPP* from the
506 western side are comparable to dense forest canopies in subtropical forests in Korea (Hong et al., 2019b),
507 deciduous forest ecosystems (Goulden et al., 1996), and a mixed hardwood forest ecosystem (Schmid et al., 2000).

508 Our study reveals that urban forests make significant traces of air temperature and CO₂ fluxes despite their
509 relatively small area. Our key findings are that urban forests in East Asia are highly influenced by the East Asian
510 monsoon like natural forests in this region, but such influence is mitigated by artificial irrigation and fertilization
511 in urban forests. In particular, our results emphasize the importance of forest management for efficient carbon
512 uptake and evaporative cooling despite the low vegetation fraction. Furthermore, our observation study also
513 indicates that caution in soil management is necessary to reduce CO₂ emissions in urban forests, mainly resulting
514 from large soil organic carbon. We also highlight that our statistical CO₂ flux partitioning is a promising method
515 to improve our understanding of the carbon cycle in urban and suburban areas, and a more extensive study is
516 required for validation in another geographical zone.

517

518 *Acknowledgment.* This research was supported by the Korea Meteorological Administration Research and
519 Development Program under Grant KMI2021-01610 and National Research Foundation of Korea Grant from the
520 Korean Government (MSIT) (NRF-2018R1A5A1024958). All data and codes are available in Lee et al. (2021)
521 and upon request to the corresponding author (jhong@yonsei.ac.kr / <https://eapl.yonsei.ac.kr>).

522



523 **References**

- 524 Awal M. A., Ohta T., Matsumoto K., Toba T., Daikoku K., Hattori S., and coauthors: Comparing the carbon
525 sequestration capacity of temperate deciduous forests between urban and rural landscapes in central Japan. *Urban*
526 *Forestry & Urban Greening*, 9(3), 261-270, 2010.
- 527 Bae, J., and Ryu, Y.: Spatial and temporal variations in soil respiration among different land cover types under
528 wet and dry years in an urban park. *Landscape and Urban Planning*, 167, 378–385, 2017.
- 529 Ballinas, M., and Barradas, V. L.: The urban tree as a tool to mitigate the urban heat island in Mexico City: A
530 simple phenomenological model. *Journal of environmental quality*, 45(1), 157-166, 2016.
- 531 Bergeron, O., and Strachan, I. B.: CO₂ sources and sinks in urban and suburban areas of a northern mid-latitude
532 city. *Atmospheric Environment*, 45(8), 1564-1573, 2011.
- 533 Bonan, G. B.: Forests and climate change: forcings, feedbacks, and the climate benefits of forests. *Science*, 320,
534 1444-1449. 2008.
- 535 Bowler, D. E., Buyung-Ali, L., Knight, T. M., and Pullin, A. S.: Urban greening to cool towns and cities: A
536 systematic review of the empirical evidence. *Landscape and Urban Planning*, 97(3), 147-155, 2010.
- 537 Chang, C. R., Li, M. H., and Chang, S. D.: A preliminary study on the local cool-island intensity of Taipei city
538 parks. *Landscape and Urban Planning*, 80(4), 386-395, 2007.
- 539 Chiesura, A.: The role of urban parks for the sustainable city. *Landscape and Urban Planning*, 68(1), 129-138,
540 2004.
- 541 Christen, A.: Atmospheric measurement techniques to quantify greenhouse gas emissions from cities. *Urban*
542 *Climate*, 10, 241-260, 2014.
- 543 Coutts, A. M., Beringer, J., and Tapper, N. J.: Impact of increasing urban density on local climate: Spatial and
544 temporal variations in the surface energy balance in Melbourne, Australia. *Journal of Applied Meteorology and*
545 *Climatology*, 46(4), 477-493, 2007a.
- 546 Coutts, A. M., Beringer, J., and Tapper, N. J.: Characteristics influencing the variability of urban CO₂ fluxes in
547 Melbourne, Australia. *Atmospheric Environment*, 41(1), 51-62, 2007b.
- 548 Crawford, B., Grimmond, C. S. B., and Christen, A.: Five years of carbon dioxide fluxes measurements in a highly
549 vegetated suburban area. *Atmospheric Environment*, 45(4), 896-905, 2011.
- 550 Crawford, B., and Christen, A.: Spatial source attribution of measured urban eddy covariance CO₂ fluxes.
551 *Theoretical and Applied Climatology*, 119(3-4), 733-755, 2015.
- 552 Emmel, C., D'Odorico, P., Revill, A., Hörtnagl, L., Ammann, C., Buchmann, N. and Eugster, W.: Canopy
553 photosynthesis of six major arable crops is enhanced under diffuse light due to canopy architecture. *Global Change*
554 *Biology*, 26(9), 2020.
- 555 Falge, E., Baldocchi, D., Olson, R., Anthoni, P., Aubinet, M., Bernhofer, C., Burba, G., Ceulemans, R., Clement,
556 R., Dolman, H., Granier, A., Gross, P., Grünwald, T., Hollinger, D., Jensen, N., Katul, G., Keronen, P., Kwalski,
557 A., Lai, C., Law, B., Meyers, T., Moncrieff, J., Moors, E., Munger, W., Pilegaard, K., Rannik, Ü., Rebmann, C.,
558 Suyker, A., Tenhunen, J., Tu, K., Verma, S., Vesala, T., Wilson, K., and Wofsy, S.: Gap filling strategies for long
559 term energy flux data sets. *Agricultural and Forest Meteorology*, 107, 71-77, 2001.



- 560 Feigenwinter, C., Vogt, R., and Christen, A.: Eddy covariance measurements over urban areas. In *Eddy*
561 *Covariance* (pp. 377-397). Springer, Dordrecht, 2012.
- 562 Feyisa, G. L., Dons, K., and Meilby, H.: Efficiency of parks in mitigating urban heat island effect: An example
563 from Addis Ababa. *Landscape and Urban Planning*, 123, 87-95, 2014.
- 564 Fratini, G., Ibrom, A., Arriga, N., Burba, G., and Papale, D.: Relative humidity effects on water vapour fluxes
565 measured with closed-path eddy-covariance systems with short sampling lines. *Agricultural and Forest*
566 *Meteorology*, 165, 53-63, 2012.
- 567 Goulden, M. L., Munger, J. W., Fan, S. M., Daube, B. C., and Wofsy, S. C.: Measurements of carbon sequestration
568 by long-term eddy covariance: Methods and a critical evaluation of accuracy. *Global Change Biology*, 2(3), 169-
569 182, 1996.
- 570 Haaland, C., and van Den Bosch, C. K.: Challenges and strategies for urban green-space planning in cities
571 undergoing densification: A review. *Urban forestry & Urban Greening*, 14(4), 760-771, 2015.
- 572 Hamada, S., and Ohta, T.: Seasonal variations in the cooling effect of urban green areas on surrounding urban
573 areas. *Urban Forestry & Urban Greening*, 9(1), 15-24, 2010.
- 574 Hansen, J., Ruedy, R., Sato, M., and Lo, K.: Global surface temperature change. *Reviews of Geophysics*, 48(4),
575 2010.
- 576 Hsieh, C. I., Katul, G., and Chi, T. W.: An approximate analytical model for footprint estimation of scalar fluxes
577 in thermally stratified atmospheric flows. *Advances in Water Resources*, 23(7), 765-772, 2000.
- 578 Hiller, R. V., McFadden, J. P., and Kljun, N.: Interpreting CO₂ fluxes over a suburban lawn: the influence of
579 traffic emissions. *Boundary-Layer Meteorology*, 138(2), 215-230, 2011.
- 580 Hong, J., and Kim, J.: Impact of the Asian monsoon climate on ecosystem carbon and water exchanges: a wavelet
581 analysis and its ecosystem modeling implications. *Global Change Biology*, 17(5), 1900-1916, 2011.
- 582 Hong, J., Takagi, K., Ohta, T., and Kodama, Y.: Wet surface resistance of forest canopy in monsoon Asia:
583 Implications for eddy-covariance measurement of evapotranspiration. *Hydrological Processes*, 28(1), 37-42, 2014.
- 584 Hong, J. W., Hong, J., Lee, S. E., and Lee, J.: Spatial distribution of urban heat island based on local climate zone
585 of automatic weather station in Seoul metropolitan area. *Atmosphere*, 23(4), 413-424, 2013.
- 586 Hong, J. W., and Hong, J.: Changes in the Seoul metropolitan area urban heat environment with residential
587 redevelopment. *Journal of Applied Meteorology and Climatology*, 55(5), 1091-1106, 2016.
- 588 Hong, J. W., Hong, J., Kwon, E. E., and Yoon, D.: Temporal dynamics of urban heat island correlated with the
589 socio-economic development over the past half-century in Seoul, Korea. *Environmental Pollution*, 254, 112934,
590 2019a.
- 591 Hong, J.-W., Hong, J. Chun, J., Lee, Y., Chang, L., Lee, J., Yi, K., Park, Y., Byun, B., and Joo, S.: Comparative
592 assessment of net CO₂ exchange across an urbanization gradient in Korea based on in situ observation, *Carbon*
593 *Balance and Management*, <https://doi.org/10.1186/s13021-019-0128-6>, 2019b.
- 594 Hong, J. W., Lee, S. D., Lee, K., and Hong, J.: Seasonal variations in the surface energy and CO₂ flux over a high-
595 rise, high-population, residential urban area in the East Asian monsoon region. *International Journal of*
596 *Climatology*, <https://doi.org/10.1002/joc.6463>, 2020.



- 597 Horst, T. W., and Lenschow, D. H.: Attenuation of scalar fluxes measured with spatially-displaced sensors.
598 *Boundary-Layer Meteorology*, 130(2), 275-300, 2009.
- 599 Kennedy, C. A., Ibrahim, N., and Hoornweg, D.: Low-carbon infrastructure strategies for cities. *Nature Climate*
600 *Change*, 4(5), 343, 2014.
- 601 Kent, C. W., Lee, K., Ward, H. C., Hong, J. W., Hong, J., Gatey, D., and Grimmond, S.: Aerodynamic roughness
602 variation with vegetation: analysis in a suburban neighbourhood and a city park. *Urban Ecosystems*, 21(2), 227-
603 243, 2018.
- 604 Khatun, R., Ohta, T., Kotani, A., Asanuma, J., Gamo, M., Han, S., Hirano, T., Nakai, Y., Saigusa, N., Takagi, K.
605 and Wang, H. (2011) Spatial variations in evapotranspiration over East Asian forest sites. I. Evapotranspiration
606 and decoupling coefficient. *Hydrological Research Letters*, 5, 83-87, 2011.
- 607 Kim, Y., Woo, S.K., Park, S., Kim, M. and Han, D.: A Study on Evaluation Methodology of Greenhouse Gas and
608 Air Pollutant Emissions on Road Network - Focusing on Evaluation Methodology of CO₂ and NO_x Emissions
609 from Road. Korea: The Korea Transport Institute (Annual Report), 2011.
- 610 Kirschbaum, M.U.F., Eamus, D., Gifford, R.M., Roxburgh, S.H. and Sands, P.J.: Definitions of some ecological
611 terms commonly used in carbon accounting. In *Net Ecosystem Exchange Workshop*, 18-20, 2001.
- 612 Kroeger, T., McDonald, R. I., Boucher, T., Zhang, P., and Wang, L.: Where the people are: Current trends and
613 future potential targeted investments in urban trees for PM₁₀ and temperature mitigation in 27 US cities.
614 *Landscape and Urban Planning*, 177, 227-240, 2018.
- 615 Kordowski, K., and Kuttler, W.: Carbon dioxide fluxes over an urban park area. *Atmospheric Environment*, 44(23),
616 2722-2730, 2010.
- 617 Kwon, H., Park, T. Y., Hong, J., Lim, J. H., and Kim, J.: Seasonality of Net Ecosystem Carbon Exchange in Two
618 Major Plant Functional Types in Korea. *Asia-Pacific Journal of Atmospheric Sciences*, 45(2), 149-163, 2009.
- 619 Lee, K. Energy, water and CO₂ exchanges in an artificially constructed urban forest, Master Degree Dissertation,
620 Yonsei University, Seoul, 2015.
- 621 Lee, K., Hong, J. W., Kim, J., and Hong, J.: Partitioning of net CO₂ exchanges at the city-atmosphere interface
622 into biotic and abiotic components. *MethodsX*, 8, 101231, 2021.
- 623 Lietzke, B., Vogt, R., Feigenwinter, C., and Parlow, E.: On the controlling factors for the variability of carbon
624 dioxide flux in a heterogeneous urban environment. *International Journal of climatology*, 35(13), 3921-3941, 2015.
- 625 Macdonald, R. W., Griffiths, R. F., and Hall, D. J.: An improved method for the estimation of surface roughness
626 of obstacle arrays. *Atmospheric Environment*, 32(11), 1857-1864, 1998.
- 627 Mahecha, M. D., Reichstein, M., Carvalhais, N., Lasslop, G., Lange, H., Seneviratne, S. I., Vargas, R., Ammann,
628 C., Arain, M. A., Cescatti, A., Janssens, I., Migliavacca, M., Montagnani, L., and Richardson, A.: Global
629 convergence in the temperature sensitivity of respiration at ecosystem level. *Science*, 329(5993), 838-840, 2010.
- 630 McCarthy, M. P., Best, M. J., and Betts, R. A.: Climate change in cities due to global warming and urban effects.
631 *Geophysical Research Letters*, 37(9), 2010.
- 632 Menzer, O., and McFadden, J. P.: Statistical partitioning of a three-year time series of direct urban net CO₂ flux
633 measurements into biogenic and anthropogenic components. *Atmospheric Environment*, 170, 319-333, 2017.



- 634 Moncrieff, J., Clement, R., Finnigan, J., and Meyers, T.: Averaging, detrending, and filtering of eddy covariance
635 time series. In *Handbook of micrometeorology*, Springer, Dordrecht, 2004.
- 636 Moriwaki, R., and Kanda, M.: Seasonal and diurnal fluxes of radiation, heat, water vapor, and carbon dioxide
637 over a suburban area. *Journal of Applied Meteorology*, 43(11), 1700-1710, 2004.
- 638 Munger, J. W., Loeschner, H. W., and Luo, H.: Measurement, tower, and site design considerations. In *Eddy
639 Covariance* (pp. 21-58). Springer, Dordrecht, 2012.
- 640 Norton, B. A., Coutts, A. M., Livesley, S. J., Harris, R. J., Hunter, A. M., and Williams, N. S.: Planning for cooler
641 cities: A framework to prioritise green infrastructure to mitigate high temperatures in urban landscapes. *Landscape
642 and Urban Planning*, 134, 127-138, 2015.
- 643 Nowak, D. J.: Atmospheric carbon reduction by urban trees. *Journal of Environmental Management*, 37(3), 207-
644 217, 1993.
- 645 Nowak, D. J., Crane, D. E., Stevens, J. C., Hoehn, R. E., Walton, J. T., and Bond, J.: A ground-based method of
646 assessing urban forest structure and ecosystem services. *Agriculture and Urban Forestry*. 34 (6): 347-358., 34(6),
647 2008.
- 648 Oke, T. R.: The energetic basis of the urban heat island. *Quarterly Journal of the Royal Meteorological Society*,
649 108(455), 1-24, 1982.
- 650 Oke, T. R.: The micrometeorology of the urban forest. *Philosophical Transactions of the Royal Society of London*.
651 B, Biological Sciences, 324(1223), 335-349, 1989.
- 652 Oke, T. R., Johnson, G. T., Steyn, D. G., and Watson, I. D.: Simulation of surface urban heat islands under 'ideal'
653 conditions at night part 2: Diagnosis of causation. *Boundary-Layer Meteorology*, 56(4), 339-358, 1991.
- 654 Oke, T.R., Mills, G., Christen, A., Voogt, J.A.: *Urban Climates*. Cambridge University Press, U.K., 2017.
- 655 Pastorello, G., Trotta, C., Canfora, E., Chu, H., Christianson, D., Cheah, Y. W., Poindexter, C., Chen,
656 J., Elbashandy, A., Humphrey, M., Isaac, P., Polidori, D., Ribeca, A., van Ingen, C., Zhang, L., Amiro,
657 B., Ammann, C., Arain, M.A., Ardö, J., Arkebauer, T., Arndt, S.K., Arriga, N., Aubinet, M., Aurela,
658 M., Baldocchi, D., Barr, A., Beamesderfer, E., Marchesini, L.B., Bergeron, O., Beringer, J., Bernhofer,
659 C., Berveiller, D., Billesbach, D., Black, T.A., Blanken, P.D., Bohrer, G., Boike, J., Bolstad, P.V., Bonal,
660 D., Bonnefond, J.-M., Bowling, D.R., Bracho, R., Brodeur, J., Brümmer, C., Buchmann, N., Burban, B., Burns,
661 S.P., Buysse, P., Cale, P., Cavagna, M., Cellier, P., Chen, S., Chini, I. Christensen, T.R., Cleverly, J., Collalti,
662 A., Consalvo, C., Cook, B.D., Cook, D., Coursolle, C., Cremonese, E., Curtis, P.S., D'Andrea, E., da Rocha,
663 H., Dai, X., Davis, K.J., De Cinti, B., de Grandcourt, A., De Ligne, A., De Oliveira, R.C., Delpierre, N., Desai,
664 A.R., Di Bella, C.M., di Tommasi, P., Dolman, H., Domingo, F., Dong, G., Dore, S., Duce, P., Dufrêne, E., Dunn,
665 A., Dušek, J., Eamus, D., Eichelmann, U., ElKhidir, H.A.M., Eugster, W., Ewenz, C.M., Ewers, B., Famulari,
666 D., Fares, S., Feigenwinter, I., Feitz, A., Fensholt, R., Filippa, G., Fischer, M., Frank, J., Galvagno, M., Gharun,
667 M., Gianelle, D., Gielen, B., Gioli, B., Gitelson, A., Goded, I., Goeckede, M., Goldstein, A.H., Gough,
668 C.M., Goulden, M.L., Graf, A., Griebel, A., Gruening, C., Grünwald, T., Hammerle, A., Han, S., Han,
669 X., Hansen, B.U., Hanson, C., Hatakka, J., He, Y., Hehn, M., Heinesch, B., Hinko-Najera, N., Hörtnagl,
670 L., Hutley, L., Ibrom, A., Ikawa, H., Jackowicz-Korczynski, M., Janouš, D., Jans, W., Jassal, R., Jiang, S., Kato,
671 T., Khomik, M., Klatt, J., Knohl, A., Knox, S., Kobayashi, H., Koerber, G., Kolle, O., Kosugi, Y., Kotani,



- 672 A., Kowalski, A., Kruijt, B., Kurbatova, J., Kutsch, W.L., Kwon, H., Launiainen, S., Laurila, T., Law,
673 B., Leuning, R., Li, Y., Liddell, M., Limousin, J.-M., Lion, M., Liska, A.J., Lohila, A., López-Ballesteros,
674 A., López-Blanco, E., Loubet, B., Loustau, D., Lucas-Moffat, A., Lüers, J., Ma, S., Macfarlane, C., Magliulo,
675 V., Maier, R., Mammarella, I., Manca, G., Marcolla, B., Margolis, H.A., Marras, S., Massman, W., Mastepanov,
676 M., Matamala, R., Matthes, J.H., Mazzenga, F., McCaughey, H., McHugh, I., McMillan, A.M.S., Merbold,
677 L., Meyer, W., Meyers, T., Miller, S.D., Minerbi, S., Moderow, U., Monson, R.K., Montagnani, L., Moore,
678 C.E., Moors, E., Moreaux, V., Moureaux, C., Munger, J.W., Nakai, T., Neiryneck, J., Nesic, Z., Nicolini,
679 G., Noormets, A., Northwood, M., Noretto, M., Nouvellon, Y., Novick, K., Oechel, W., Olesen, J.E., Ourcival,
680 J.-M., Papuga, S.A., Parmentier, F.-J., Paul-Limoges, E., Pavelka, M., Peichl, M., Pendall, E., Phillips,
681 R.P., Pilegaard, K., Pirk, N., Posse, G., Powell, T., Prasse, H., Prober, S.M., Rambal, S., Rannik, Ü., Raz-Yaseef,
682 N., Reed, D., de Dios, V.R., Restrepo-Coupe, N., Reverter, B.R., Roland, M., Sabbatini, S., Sachs, T., Saleska,
683 S.R., Sánchez-Cañete, E.P., Sanchez-Mejia, Z.M., Schmid, H.P., Schmidt, M., Schneider, K., Schrader,
684 F., Schroder, I., Scott, R.L., Sedláč, P., Serrano-Ortíz, P., Shao, C., Shi, P., Shironya, I., Siebicke, L., Šigut,
685 L., Silberstein, R., Sirca, C., Spano, D., Steinbrecher, R., Stevens, R.M., Sturtevant, C., Suyker, A., Tagesson,
686 T., Takanaishi, S., Tang, Y., Tapper, N., Thom, J., Tiedemann, F., Tomassucci, M., Tuovinen, J.-P., Urbanski,
687 S., Valentini, R., van der Molen, M., van Gorsel, E., van Huissteden, K., Varlagin, A., Verfaillie, J., Vesala,
688 T., Vincke, C., Vitale, D., Vygodskaya, N., Walker, J.P., Walter-Shea, E., Wang, H., Weber, R., Westermann,
689 S., Wille, C., Wofsy, S., Wohlfahrt, G., Wolf, S., Woodgate, W., Li, Y., Zampedri, R., Zhang, J., Zhou, G., Zona,
690 D., Agarwal, D., Biraud, S., Torn, M., and Papale, D.: The FLUXNET2015 dataset and the ONEFlux processing
691 pipeline for eddy covariance data. *Scientific Data*, 7(1), 1-27, 2020.
- 692 Pataki, D. E., Bowling, D. R., and Ehleringer, J. R.: Seasonal cycle of carbon dioxide and its isotopic composition
693 in an urban atmosphere: Anthropogenic and biogenic effects. *Journal of Geophysical Research: Atmospheres*, 108,
694 D23, <https://doi.org/10.1029/2003JD003865>, 2003.
- 695 Peters, E. B., and McFadden, J. P.: Continuous measurements of net CO₂ exchange by vegetation and soils in a
696 suburban landscape. *Journal of Geophysical Research: Biogeosciences*, 117, G3,
697 <https://doi.org/10.1029/2011JG001933>, 2012.
- 698 Piao, S., Luyssaert, S., Ciais, P., Janssens, I. A., Chen, A., Cao, C., Fang, J., Friedlingstein, P., Luo, Y., and Wang,
699 S.: Forest annual carbon cost: A global-scale analysis of autotrophic respiration. *Ecology*, 91(3), 652-661, 2010.
- 700 Rahmstorf, S., and Coumou, D.: Increase of extreme events in a warming world. *Proceedings of the National
701 Academy of Sciences*, 108(44), 17905-17909, 2011.
- 702 Randerson, J.T., Chapin Iii, F.S., Harden, J.W., Neff, J.C. and Harmon, M.E.: Net ecosystem production: a
703 comprehensive measure of net carbon accumulation by ecosystems. *Ecological Applications*, 12(4), 937-947,
704 2002.
- 705 Raupach, M. R., Antonia, R. A., and Rajagopalan, S.: Rough-wall turbulent boundary layers, *Applied Mechanics
706 Reviews*, 44(1), 1-25, 1991.
- 707 Rowntree, R. A., and Nowak, D. J.: Quantifying the role of urban forests in removing atmospheric carbon dioxide.
708 *Journal of Arboriculture*. 17 (10): 269-275., 17(10), 1991.



- 709 Roy, S., Byrne, J., and Pickering, C.: A systematic quantitative review of urban tree benefits, costs, and assessment
710 methods across cities in different climatic zones. *Urban Forestry and Urban Greening*, 11(4), 351-363, 2012.
- 711 Schmid, H. P., Grimmond, C. S. B., Cropley, F., Offerle, B., and Su, H. B.: Measurements of CO₂ and energy
712 fluxes over a mixed hardwood forest in the mid-western United States. *Agricultural and Forest Meteorology*,
713 103(4), 357-374, 2000.
- 714 Schmid, H. P., Su, H. B., Vogel, C. S., and Curtis, P. S.: Ecosystem-atmosphere exchange of carbon dioxide over
715 a mixed hardwood forest in northern lower Michigan. *Journal of Geophysical Research: Atmospheres*, 108(D14),
716 2003.
- 717 Shashua-Bar, L., and Hoffman, M. E.: Vegetation as a climatic component in the design of an urban street: An
718 empirical model for predicting the cooling effect of urban green areas with trees. *Energy and Buildings*, 31(3),
719 221-235, 2000.
- 720 Shim, C., J. Hong, J. Hong, Y. Kim, M. Kang, B. Thakuri, Y. Kim, J. Chun: Evaluation of MODIS GPP over a
721 complex ecosystem in East Asia: A case of Gwangneung flux tower in Korea, *Advances in Space Research*, 54,
722 2296-2308, 2014.
- 723 Spronken-Smith, R. A., Oke, T. R., and Lowry, W. P.: Advection and the surface energy balance across an
724 irrigated urban park. *International Journal of Climatology: A Journal of the Royal Meteorological Society*, 20(9),
725 1033-1047. 2000.
- 726 Stagakis, S., Chrysoulakis, N., Spyridakis, N., Feigenwinter, C., and Vogt, R.: Eddy Covariance measurements
727 and source partitioning of CO₂ emissions in an urban environment: Application for Heraklion, Greece.
728 *Atmospheric Environment*, 201, 278-292, 2019.
- 729 Stewart, I. D.: A systematic review and scientific critique of methodology in modern urban heat island literature.
730 *International Journal of Climatology*, 31(2), 200-217, 2011.
- 731 Stewart, I. D., and Oke, T. R.: Local climate zones for urban temperature studies. *Bulletin of the American
732 Meteorological Society*, 93(12), 1879-1900, 2012.
- 733 Stoy, P. C., Katul, G. G., Siqueira, M. B., Juang, J. Y., Novick, K. A., Uebelherr, J. M., and Oren, R.: An evaluation
734 of models for partitioning eddy covariance-measured net ecosystem exchange into photosynthesis and respiration.
735 *Agricultural and Forest Meteorology*, 141(1), 2-18, 2006.
- 736 Suyker, A.E. and Verma, S.B.: Interannual water vapor and energy exchange in an irrigated maize-based
737 agroecosystem. *Agricultural and Forest Meteorology*, 148, 417-427, 2008.
- 738 Takanashi, S., Kosugi, Y., Tanaka, Y., Yano, M., Katayama, T., Tanaka, H., and Tani, M.: CO₂ exchange in a
739 temperate Japanese cypress forest compared with that in a cool-temperate deciduous broad-leaved forest.
740 *Ecological Research*, 20(3), 313-324, 2005.
- 741 Ueyama, M., and Ando, T.: Diurnal, weekly, seasonal, and spatial variabilities in carbon dioxide flux in different
742 urban landscapes in Sakai, Japan. *Atmospheric Chemistry and Physics*, 16(22), 14727-14740, 2016.
- 743 United Nations, Department of Economic and Social Affairs, Population Division: *World Urbanization Prospects:
744 The 2018 Revision (ST/ESA/SER.A/420)*. New York: United Nations, 2019.
- 745 Velasco, E., and Roth, M.: Cities as net sources of CO₂: Review of atmospheric CO₂ exchange in urban
746 environments measured by eddy covariance technique. *Geography Compass*, 4(9), 1238-1259, 2010.



- 747 Velasco, E., Roth, M., Tan, S. H., Quak, M., Nabarro, S. D. A., and Norford, L.: The role of vegetation in the
748 CO₂ flux from a tropical urban neighbourhood, *Atmospheric Chemistry and Physics*, 13, 10185–10202,
749 <https://doi.org/10.5194/acp-13-10185-2013>, 2013.
- 750 Velasco, E., Roth, M., Norford, L., and Molina, L. T.: Does urban vegetation enhance carbon sequestration?,
751 *Landscape and Urban Planning*, 148, 99-107, 2016.
- 752 Vickers, D., and Mahrt, L.: Quality control and flux sampling problems for tower and aircraft data. *Journal of*
753 *Atmospheric and Oceanic Technology*, 14(3), 512-526, 1997.
- 754 Wang, L., Lee, X., Schultz, N., Chen, S., Wei, Z., Fu, C., Gao, Y., Yang, Y., and Lin, G.: Response of surface
755 temperature to afforestation in the Kubuqi Desert, Inner Mongolia. *Journal of Geophysical Research:*
756 *Atmospheres*, 123, 948-964, 2018.
- 757 Ward, H. C., Evans, J. G., and Grimmond, C. S. B.: Multi-season eddy covariance observations of energy, water
758 and carbon fluxes over a suburban area in Swindon, UK. *Atmospheric Chemistry and Physics*, 13(9), 4645-4666,
759 2013.
- 760 Ward, H. C., Kotthaus, S., Grimmond, C. S. B., Bjarkegren, A., Wilkinson, M., Morrison, W. T. J., Evans, J. G.,
761 Morrison, J. I. L. M and Iamarino, M.: Effects of urban density on carbon dioxide exchanges: Observations of dense
762 urban, suburban and woodland areas of southern England. *Environmental Pollution*, 198, 186-200, 2015.
- 763 Weissert, L. F., Salmond, J. A., and Schwendenmann, L.: A review of the current progress in quantifying the
764 potential of urban forests to mitigate urban CO₂ emissions. *Urban Climate*, 8, 100-125, 2014.
- 765 Yu, C., and Hien, W. N.: Thermal benefits of city parks. *Energy and Buildings*, 38(2), 105-120, 2006.
- 766



767 Table 1. Details of the stations used in this study.

Sites	Location	LCZ	Height [m]	Used variables
Eddy covariance station				
SFP (Seoul Forest Park)	37.5446°N, 127.0379°E	LCZ _A	12.2	
EP (Eunpyeong)	37.6350°N, 126.9287°E	LCZ ₁	30	<i>Flux</i>
Automatic weather station				
SD (Seongdong)	37.5472°N, 127.0389°E	LCZ _{5B}	25	<i>T_{air}, RH, WS, WD, Precipitation</i>
AVG				
(Gangnam)	37.5134°N, 127.0467°E	LCZ ₂₁	59	
(Seocho)	37.4889°N, 127.0156°E	LCZ ₂₁	35.5	<i>T_{air}</i>
(Songpa)	37.5115°N, 127.0967°E	LCZ ₁₅	58.2	
Aerodrome meteorological observation station				
GP (Gimpo)	37.5722°N, 126.7751°E	LCZ _D	11.4	<i>T_{air}</i>

768

769



770 Table 2. Gap-filled annual budgets for surface energy fluxes and precipitation (P).

Sites	ET (mm)	Q_H (MJ m ⁻²)	Q_E (MJ m ⁻²)	Q^* (MJ m ⁻²)	P (mm)
1 st year (2013.06 – 2014.05)	367	726	896	1797	1256
2 nd year (2014.06 – 2015.05)	320	867	781	1848	932
Mean annual sum of two-year	344	797	839	1823	1094

771

772



773 Table 3. Gap-filled annual budgets for F_C (observed by EC measurement) and its components, indicating
774 ecosystem respiration (RE), photosynthetic uptake by vegetation (GPP), vehicle emissions (E_R), and building
775 emissions (E_B). All fluxes are in $\text{kg CO}_2 \text{ m}^{-2} \text{ year}^{-1}$.

Sites	F_C	RE	GPP	E_R	E_B
1 st year (2013.06 – 2014.05)	6.6	5.1 (71%)	4.7 (64%)	3.3 (76%)	1.0 (20%)
2 nd year (2014.06 – 2015.05)	7.6	5.0 (77%)	4.5 (70%)	3.2 (81%)	1.9 (15%)
Mean annual sum of two-year	7.1	5.1 (65%)	4.6 (59%)	3.3 (71%)	1.5 (25%)

776

777

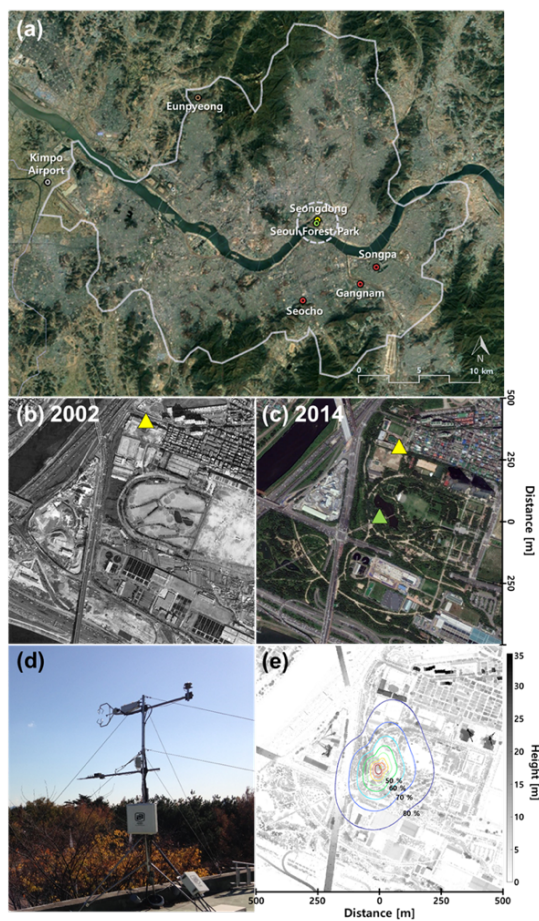


778 Table 4. Annual budgets of biogenic F_C components and ratios in deciduous broadleaf forests in similar climatic
 779 conditions reported in previous studies. All fluxes are in $\text{kg CO}_2 \text{ m}^{-2} \text{ year}^{-1}$.

Sites name	Reference	MAT (°C)	MAP (mm)	maximum LAI	<i>RE</i>	<i>GPP</i>	<i>NBE</i>	<i>RE/GPP</i>
Seoul Forest Park	This study	13.9	1094	1.6	5.1	4.6	+0.5	1.11
Nagoya urban forest	Awal et al. (2010)	15.9	1680	5.5	4.9	6.2	-1.3	0.74
Toyota rural forest		14.5	1518	4.5	2.6	4.6	-2.0	0.56
Gwangneung deciduous forest	Kwon et al. (2010)	12.8	1487	5	3.8	4.1	-0.3	0.93
Kiryu Experimental Watershed	Takanashi et al. (2005)	14.1	1309	5.5	3.9	5.6	-1.7	0.70
FLUXNET2015 dataset*	Pastorello et al. (2020)	14.5	1113		4.1	6.0	-1.9	0.68

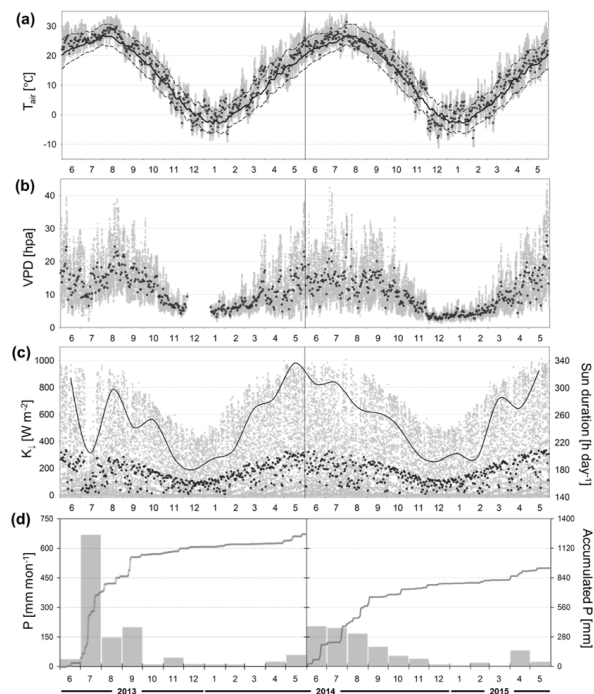
780 *Average value of 8-year data from 4 sites having mean annual temperature (MAT) of 12-16°C, mean annual
 781 precipitation (MAP) of 900-2000 mm.

782



783

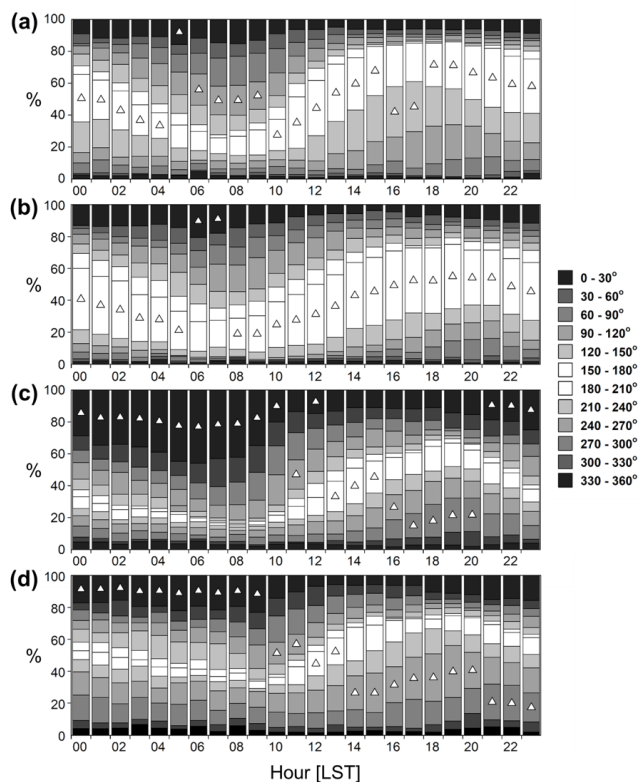
784 Figure 1. Site descriptions. (a) Location of the stations in Seoul (modified from map data © Google Earth 2019),
785 (b) aerial photographs around Seoul Forest Park (SFP) in 2002 before the creation of the park and (c) in 2014
786 during the observation period (SFP; *green triangle*, SD; *yellow triangle*), (d) photograph of the SFP station, and
787 (e) footprint climatology (Hsieh et al., 2000) with the height of surrounding obstacles around the SFP station.



788

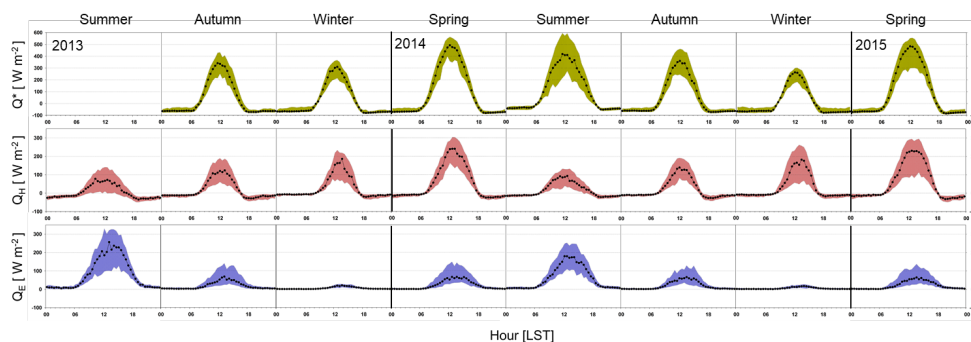
789 Figure 2. Climatic conditions of the SFP for two years from June 2013 to May 2015: 30-min (*gray dots*) and daily
790 mean (*black dots*) (a) air temperature with 30-year normal values of Seoul (daily mean; *solid line*, min and max;
791 *dashed lines*), (b) vapor pressure deficit (VPD) and missing data existing on December 2013, (c) downward
792 shortwave radiation (K_i) and monthly averaged sunshine duration per day (*black line*), (d) monthly precipitation
793 (*gray bars*) and yearly accumulated precipitation (*solid line*).

794



795

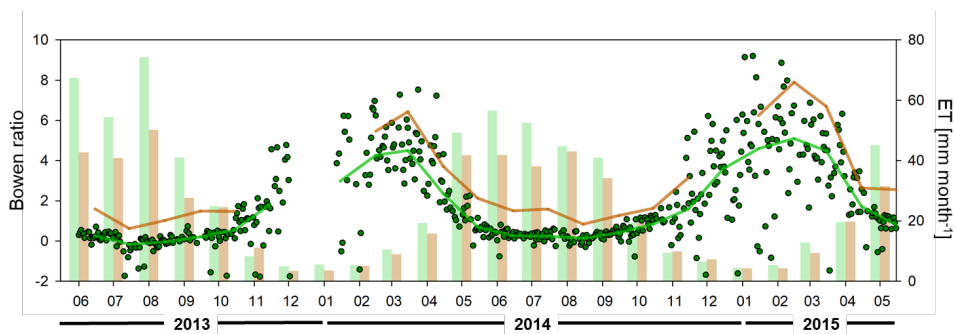
796 Figure 3. Seasonal mean diurnal courses of wind direction for 30° intervals. Each column represents the hourly
797 ratio of the wind direction of the season: (a) spring (b) summer (c) autumn (d) winter. The white triangle indicates
798 the dominant wind direction during that hour.



799

800 Figure 4. Diurnal variations of surface energy fluxes. Seasonal median diurnal variations (*points*) and interquartile
801 ranges (*shaded*) of 30-min sensible heat flux (Q_H), latent heat flux (Q_E), and net radiation (Q^*) for two years.
802 Since the net radiation system was installed in September 2013, there was no Q^* value in the first summer.

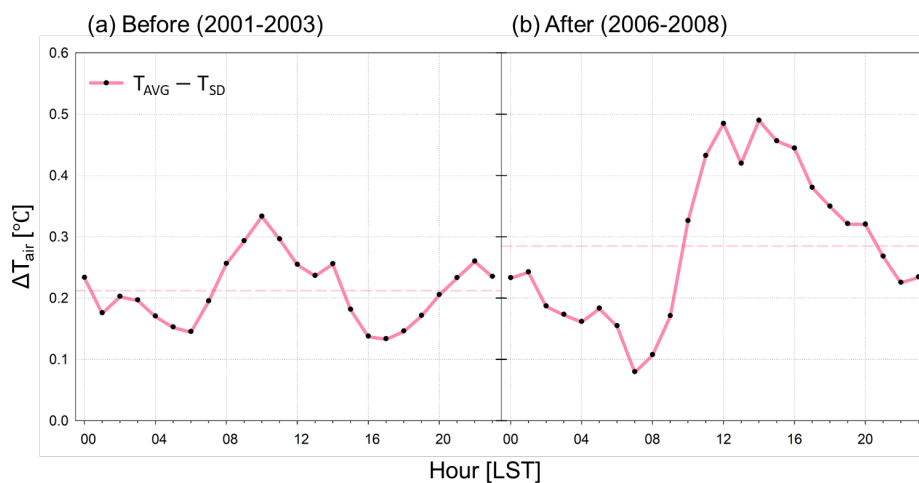
803



804

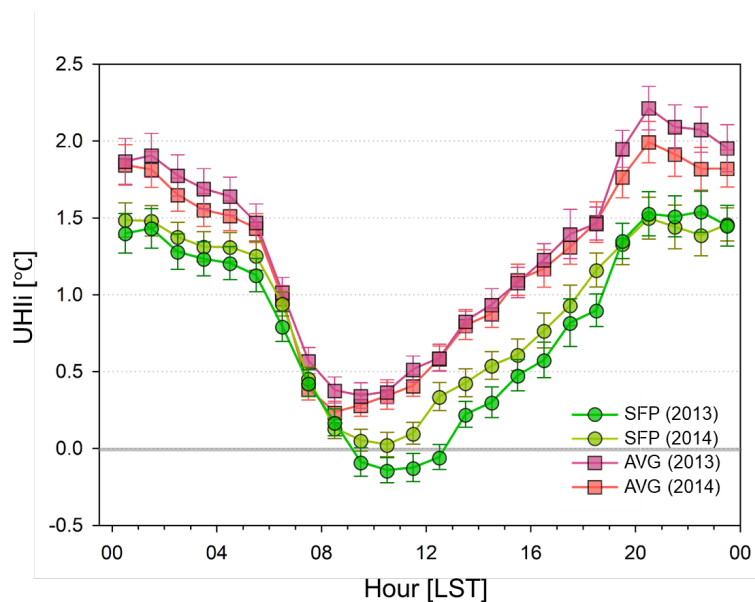
805 Figure 5. Daily Bowen ratio ($\beta = \sum Q_H / \sum Q_E$; dots), monthly Bowen ratio (lines), and gap-filled monthly
806 evapotranspiration (ET; bars) for two years (SFP; green, EP; brown).

807



808

809 Figure 6. Mean diurnal pattern of air temperature difference (ΔT_{air}) between AVG and SD (a) before and (b) after
810 the construction of the park in summer. AVG indicates an average of three automatic weather stations (Gangnam,
811 Seocho, Songpa) in Seoul. The red dash line indicates the mean ΔT_{air} before and after the construction of the park.



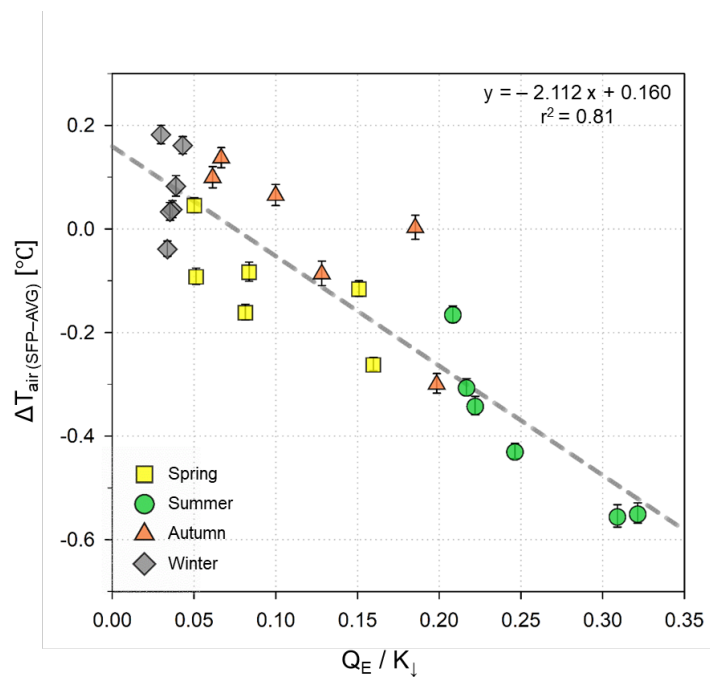
812

813 Figure 7. Hourly mean diurnal variation of the urban heat island intensity (UHli) of the SFP and AVG in the
814 summer of 2013 and 2014. The error bars represent standard errors.

815

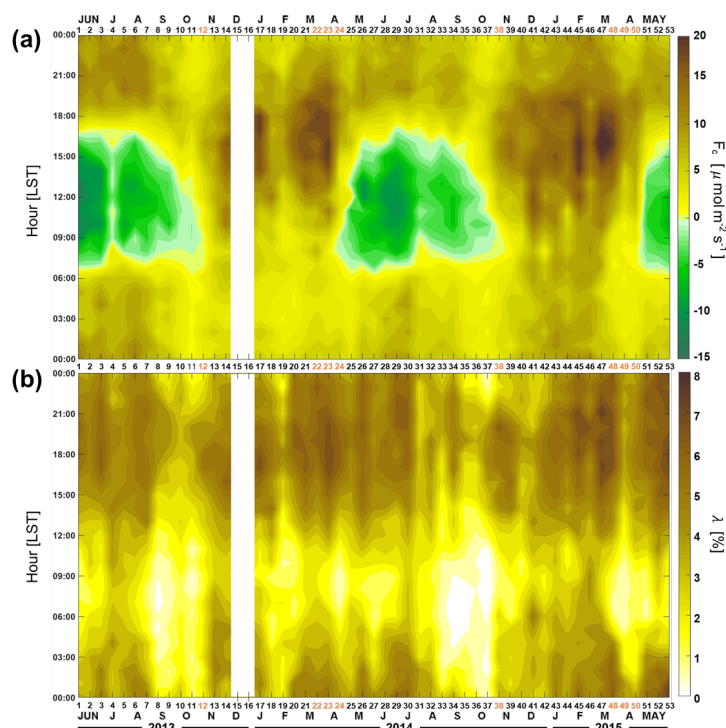


816



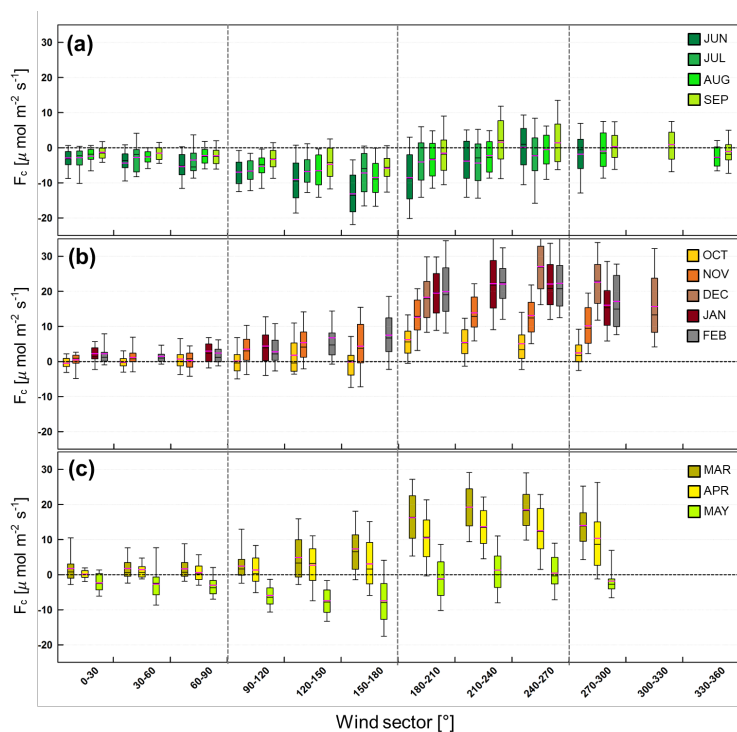
817

818 Figure 8. Relationship between the ratio of monthly Q_E to K_l and mean air temperature difference between SFP
819 and AVG during the daytime ($K_l > 120 \text{ W m}^{-2}$) for two years. The error bars represent standard errors.



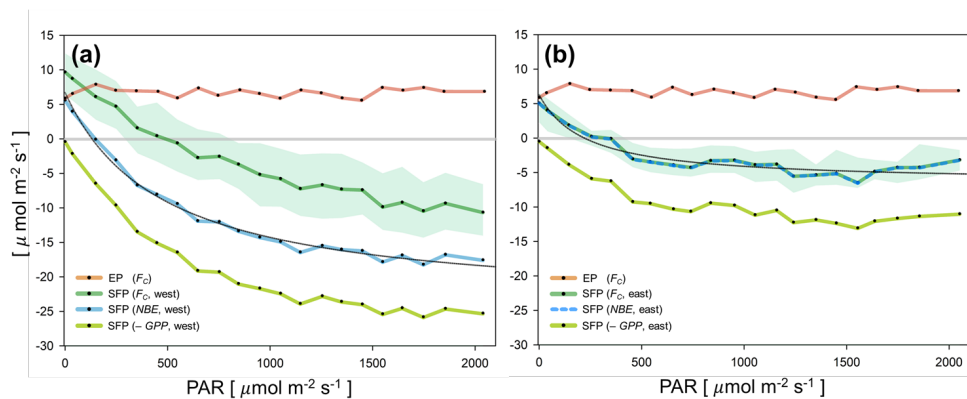
820

821 Figure 9. (a) Temporal variation of hourly averaged F_C and (b) source area weighted road fraction (λ) for every
822 two-week. The horizontal axis indicates the order of every two-week for two years, and the vertical axis is the
823 time of day. In December 2013, there was a gap for approximately 4 weeks due to the power system failure. The
824 yellow numbers indicate the two-week (12th, 22nd–24th, 38th, and 48th–50th) having the transition period when the
825 observed F_C is primarily attributable to traffic emissions (E_R).



826

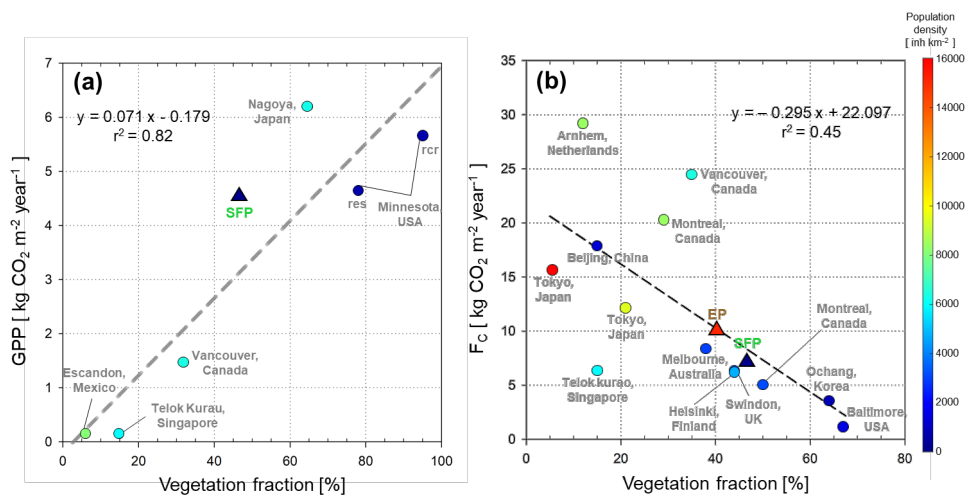
827 Figure 10. Monthly boxplots of daytime ($K_1 > 120 \text{ W m}^{-2}$) F_c by wind direction. Boxes have a minimum of 20
828 samples. Box limits are upper and lower quartiles, and whiskers are distances of 1.5 times the interquartile range
829 from each quartile. Median and mean values are indicated by the black and pink horizontal lines.



830

831 Figure 11. During the growing season (June–August 2013, 2014), light-response curves as a function of
832 photosynthetically active radiation (PAR, in bins of $100 \mu\text{mol m}^{-2} \text{s}^{-1}$): (a) for the western sectors ($150^\circ < \Phi <$
833 300°) and (b) for the eastern sectors ($30^\circ < \Phi < 90^\circ$). Black line is a rectangular hyperbolic equation fitting net
834 biome exchange ($NBE = RE - GPP = F_C - E_R$) to PAR, and EP (brown line) is a light-response curve for the
835 high-rise high-population residential area in Seoul. The shaded areas indicate interquartile range.

836



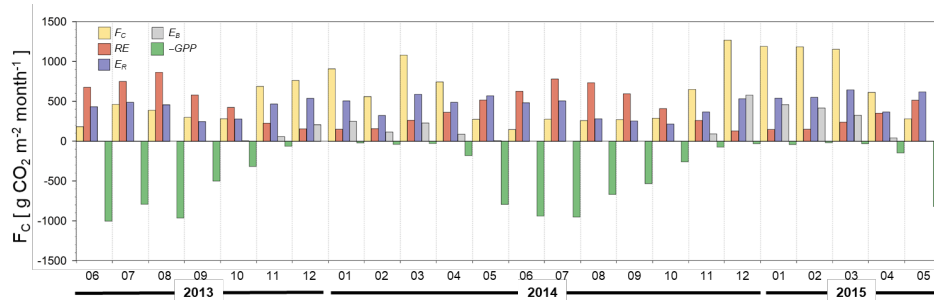
837

838 Figure 12. Relationship between vegetation fraction (a) annual *GPP* and (b) annual *F_c* in urban sites (Fig. 12a in
839 Hong et al., 2019b).

840



841
842



843
844

845 Figure 13. Monthly sums for gap-filled F_c (yellow bar) with RE (red bar), E_R (blue bar), E_B (gray bar), and –
846 GPP (green bar)
847